

# The Cartesian Shortcut: Re-evaluate Vision Reasoning in Polar Coordinate Space

Xia Hu<sup>1</sup>, Zhenrui Yue<sup>1</sup>, Brian Potetz<sup>1</sup>, Howard Zhou<sup>1</sup>, Leonidas Guibas<sup>1,2</sup>, Chun-Ta Lu<sup>3</sup> and Zhicheng Wang<sup>1</sup>

<sup>1</sup>Google DeepMind, <sup>2</sup>Stanford University, <sup>3</sup>Google Research

As current Multimodal Large Language Models rapidly saturate canonical visual reasoning benchmarks, a key question emerges: do these strong scores genuinely reflect robust visual understanding? We identify a pervasive vulnerability, the Cartesian Shortcut: visual reasoning benchmarks prevalently build on orthogonal grid-based layouts that can be readily discretized into explicit textual coordinates. Models systematically exploit this property, heavily leveraging text-based deductive reasoning to assist visual problem-solving. To systematically dismantle this shortcut, we introduce **Polaris-Bench**, which re-formulates 53 visual reasoning tasks in Polar coordinate space with paired Cartesian counterparts as reference, while preserving consistent logical constraints and task semantics—thus fundamentally breaking the orthogonal prior that models exploit. Comprehensive evaluation across 14 state-of-the-art MLLMs reveals that frontier models achieving 70–83% on Cartesian layouts collapse to 31–39% on Polar equivalents, with degradation persisting even under complete logical equivalence. Moreover, reasoning gains observed on Cartesian layouts are severely diminished on Polar equivalents. These findings expose a critical deficiency in current MLLMs: the lack of topology-invariant visual reasoning.

## 1. Introduction

Recent Multimodal Large Language Models (MLLMs) [2, 16, 24, 27] achieve remarkable, often human-level performance across canonical visual reasoning benchmarks [6, 18, 30, 41]. However, as these datasets rapidly saturate, a critical question emerges: have models genuinely acquired visual reasoning abilities, or are they merely exploiting text-based heuristics [4, 7, 20, 38]? In this study, we expose a pervasive systemic vulnerability that creates an illusion of profound visual capability: **the Cartesian Shortcut**.

Orthogonal grid-based layouts, which underlie many prominent visual reasoning benchmarks, can be readily discretized into explicit textual coordinates. We find that MLLMs systematically exploit this property: across a synthetic subset of 9 prominent benchmarks (e.g., [18, 19]), frontier models explicitly invoke Cartesian coordinates (e.g., “row 2”, “(x,y)”) in over 56% of intermediate Chain-of-Thought [34] reasoning, converting visual layouts into textual representations to assist problem-solving. By substantially offloading reasoning from visual perception to text-based deduction, this shortcut significantly confounds the evaluation of visual reasoning on grid-based testbeds.

Crucially, this shortcut collapses once the orthogonal layout is distorted: on a logically identical Sudoku puzzle rendered in Polar coordinates, frontier models that correctly solve the Cartesian version fail on its topological equivalent (Figure 1). Drawing on this observation, we introduce **Polaris-Bench**, comprising 53 procedurally generated visual reasoning tasks in Polar coordinate space, each accompanied by a Cartesian counterpart as controlled reference under consistent logical constraints. The Cartesian-to-Polar topological transformation breaks the orthogonal structure underlying the Cartesian shortcut, disrupting models’ ability to easily discretize visual layouts into textual coordinates. This design provides a controlled diagnostic testbed to re-evaluate visual reasoning under topological transformation, with the consistent logical constraints enabling direct cross-topology evaluation and analysis.

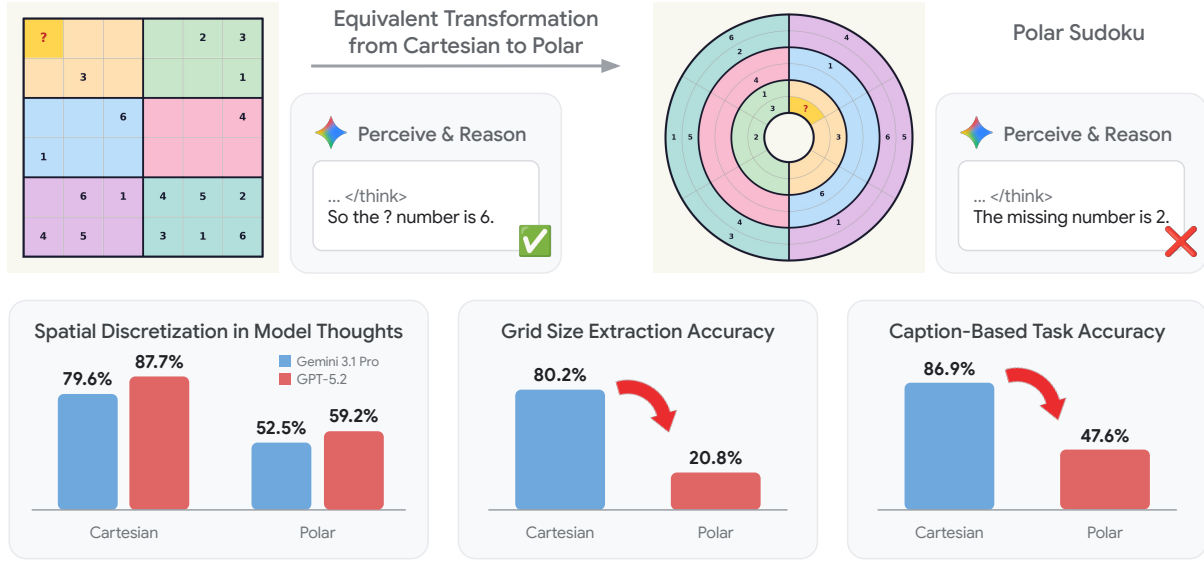


Figure 1 | Illustration and empirical evidence of the Cartesian Shortcut. (Top) An equivalent sudoku question in Cartesian and Polar spaces (row to ring, column to angular sector). The model correctly solves the orthogonal layout but fails on its topological equivalent. (Bottom Left) The percentage of intermediate CoT that explicitly invokes textual coordinates. Gemini-3.1-Pro and GPT-5.2 both exhibit high frequencies on Cartesian layouts. (Bottom Middle & Right) Two-stage perception and reasoning analysis on Gemini-3.1-Pro: grid size extraction accuracy estimates visual perception capability (Middle), while task accuracy is evaluated on correctly perceived instances (Right). High Cartesian accuracy validates the effectiveness of the shortcut, while the sharp decline on Polar layouts demonstrates that it collapses once the orthogonal structure is disrupted.

We comprehensively evaluate Polaris-Bench across 14 state-of-the-art MLLMs spanning both proprietary and open-source families. The results reveal a striking and consistent pattern that frontier models achieving 70–83% accuracy on Cartesian layouts see their performance collapse to 31–39% on Polar equivalents, with the largest degradation approaching 47 points. Critically, the degradation persists even on tasks where the transformation preserves complete logical equivalence (i.e., identical rules, constraints, and ground truths), confirming that the coordinate transformation alone suffices to disrupt model reasoning. Moreover, while enabling high reasoning mode yields substantial accuracy gains on Cartesian layouts, these gains are severely diminished on Polar equivalents.

These findings reveal a critical problem that current MLLMs lack fundamental topology-invariant visual reasoning capability. Our main contributions are as follows:

- We identify and empirically validate the Cartesian Shortcut, whereby MLLMs systematically discretize orthogonal grid-based layouts into explicit textual coordinates, offloading visual reasoning onto text-based deduction and confounding existing visual reasoning evaluation.
- We introduce Polaris-Bench, which re-formulates 53 visual reasoning tasks in Polar coordinate space to systematically disrupt the Cartesian Shortcut, with paired Cartesian counterparts enabling cross-topology evaluation.
- Our comprehensive evaluation across 14 state-of-the-art MLLMs demonstrates that topological transformation induces drastic and universal performance collapse, with degradation persisting across diverse model families, scales, and reasoning configurations.

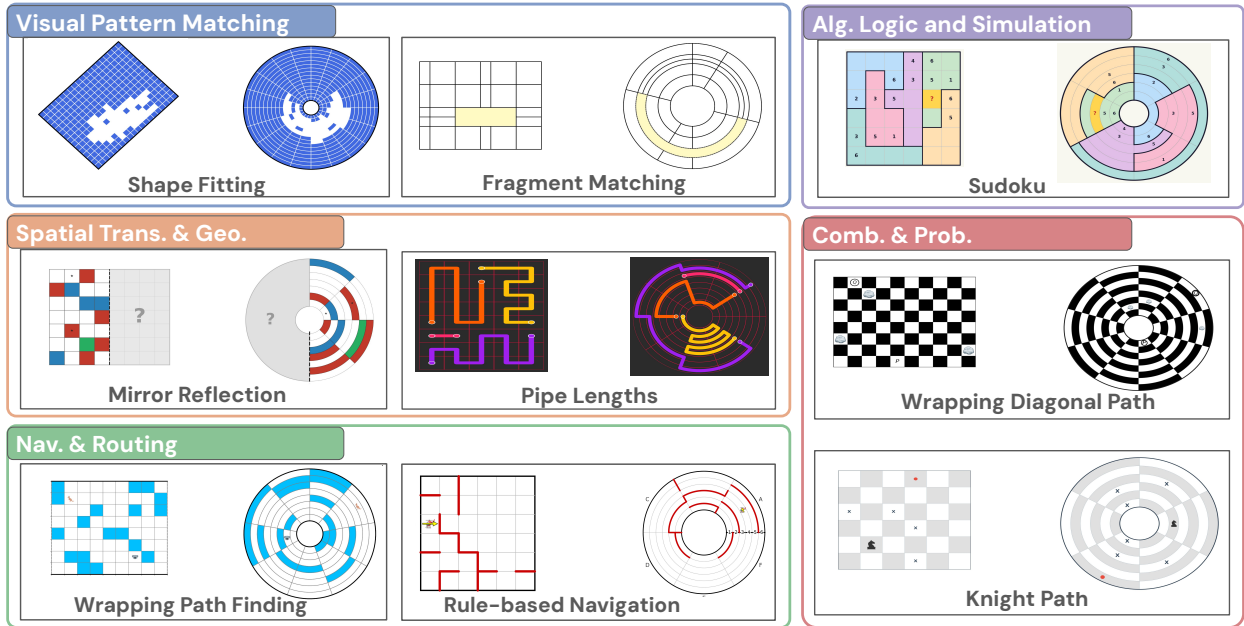


Figure 2 | Representative examples for each of the five core taxonomies in Polaris-Bench.

## 2. Rethinking vision reasoning: the Cartesian Shortcut

Current MLLMs excel on vision reasoning benchmarks, where many of these tasks are built upon synthetic, grid-based layouts [25, 28]. To investigate how models approach them, we analyzed over 3,800 synthetic-based questions across 9 prominent visual reasoning benchmarks (e.g., [18, 19]). Our Chain-of-Thought (CoT) [34] analysis reveals a striking pattern: in over 56% of these examples, frontier models (e.g., Gemini-3-Flash) explicitly discretize the input image into Cartesian coordinates, generating text such as “starting at (2,3), moving to (3,5).” By translating these visual layouts into discrete matrices, models heavily offload visual logic onto text-based deductive reasoning, thereby reducing the need for persistent visual grounding. We define this phenomenon as the **Cartesian Shortcut**. While this behavior demonstrates robust deductive capability, it exposes a critical flaw in current evaluations: models can leverage textual discretization to assist visual reasoning, projecting an inflated estimate of visual capability.

To further empirically validate this Cartesian Shortcut, we analyzed model behavior on our paired Cartesian-Polar benchmark. Intermediate CoT from frontier models reveal a deep dependency on textual discretization, explicitly invoking Cartesian coordinates in over 80% of Cartesian examples (Figure 1(left)). We further probed this dependency by a two-stage experiment on Gemini-3.1-Pro [16]. The model first generates a descriptive caption, then solves the task based on the caption. As shown in Figure 1(middle, right), the model achieves 80.2% accuracy on visual layout perception, estimated via grid dimension extraction from model-generated captions, and task accuracy on the subset of correctly perceived instances reaches 86.9%. This empirically validates that the Cartesian Shortcut is not merely a behavioral pattern but a highly effective problem-solving strategy for current MLLMs. This effectiveness raises a fundamental concern: benchmarks built on orthogonal grids may systematically overestimate visual reasoning capabilities.

Drawing on the fundamental duality of coordinate systems [3, 42], we introduce Polaris-Bench to dismantle the Cartesian shortcut. Polaris-Bench re-formulates visual reasoning tasks in Polar coordinate space, pairing each instance with a Cartesian counterpart as controlled reference. This mapping is a visual and topological transformation that preserves the underlying logical constraints,

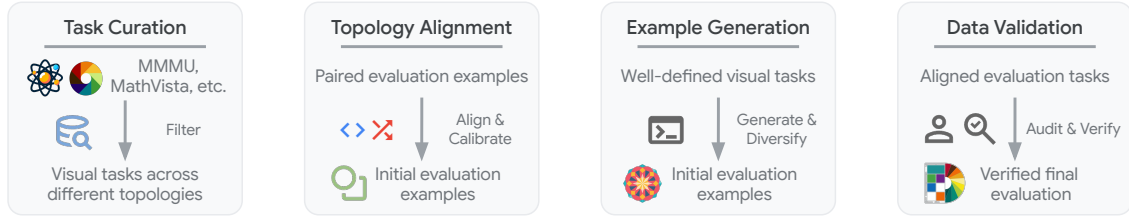


Figure 3 | An overview of the construction process of the Polaris-Bench.

rather than a mathematical translation. The spatial topological transformation breaks the orthogonal prior that underlies the Cartesian Shortcut. Applying the same two-stage analysis to Polar layouts reveals a stark contrast: visual layout perception accuracy falls to merely 20.8%, and task accuracy on correctly perceived instances to 47.6% (Figure 1). This validates the fact that the Polar transformation effectively disrupts the Cartesian shortcut: models struggle to discretize the Polar layout into text, and downstream task performance degrades accordingly.

### 3. Polaris-Bench

#### 3.1. Benchmark overview

**Polaris-Bench** comprises 53 procedurally generated visual reasoning tasks, each re-formulated in Polar coordinate space with paired Cartesian counterparts as controlled reference, yielding over 10,600 core test cases. This paired design is central to our methodology: by presenting each task in two coordinate systems that share identical rules, question context, and identical ground truths for the majority, we construct a controlled diagnostic testbed where performance differences can be directly attributed to the coordinate transformation. To ensure valid spatial logic across coordinate systems, physical concepts are contextually adapted (e.g., Cartesian grid distances are translated to unit edge counting in Polar space). All task outputs are constrained to deterministic formats (multiple-choice options, exact digits, coordinates, string, and lists) to facilitate rigorous automated evaluation.

**Topology Alignment.** The paired Cartesian-Polar evaluation introduces a design constraint: the angular dimension of Polar coordinates is inherently cyclic, with 360 wrapping seamlessly to 0. This cylindrical connectivity can alter valid solutions for adjacency-sensitive tasks, creating a potential confound between perceptual distortion and genuine topological divergence.

We address this through two boundary conditions. Under the *bounded* condition, boundary rings and radial seams act as impenetrable barriers, producing a closed Polar grid topologically equivalent to its Cartesian counterpart with identical ground truths. Under the *wrapping* condition, we preserve the natural cyclic connectivity of Polar space, retaining its intrinsic topological properties as an additional dimension of the evaluation; for a subset of these tasks, we additionally introduce cyclic boundaries in the Cartesian version (e.g., exit left will enter right) to both align ground truths and examine whether models can handle wrapping within standard grid layouts. This yields two alignment categories: the large majority are *fully aligned* where topological transformation is the only variance, while a deliberately preserved subset remains *partially aligned*, where cylindrical connectivity alters the solution space. This stratification enables controlled ablation: gaps on fully aligned tasks isolate perceptual distortion from the coordinate mapping, while gaps on partially aligned tasks additionally capture failures under altered topology.

**Task Taxonomy.** To evaluate vision reasoning across diverse cognitive dimensions, we organize the 53 tasks into five categories based on their core cognitive operation (Figure 4). *Visual Pattern Matching* (11 tasks) evaluates pattern recognition and structural discrimination within organized visual layouts. *Spatial Transformation and Geometry* (13 tasks) evaluates geometric transformation reasoning (e.g., rotation, reflection, folding) and quantitative property inference. *Navigation and Routing* (14 tasks) evaluates sequential positional state tracking, requiring models to execute or trace multi-step movements under environmental constraints. *Combinatorics and Probability* (9 tasks) evaluates systematic combinatorial enumeration and probabilistic reasoning. *Algorithmic Logic and Simulation* (6 tasks) evaluates constraint satisfaction and deterministic forward simulation. This categorization enables fine-grained analysis of how the Cartesian Shortcut differentially affects distinct reasoning capabilities.

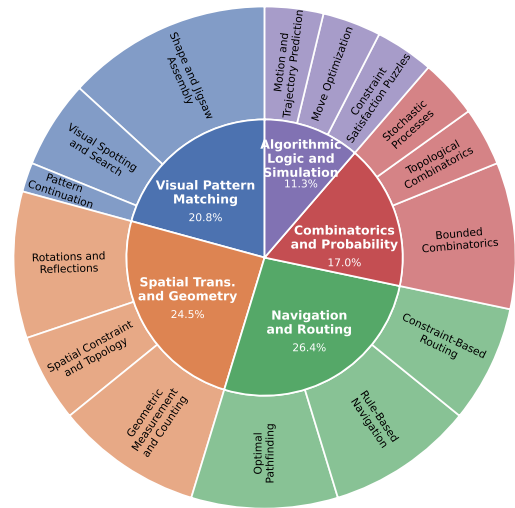


Figure 4 | Distribution of 53 tasks across the five core categories.

### 3.2. Benchmark construction

Given the scarcity of Polar tasks in the wild, we systematically generated our benchmark data instead of collecting it manually. Specifically, we synthesize Polaris-Bench through a four-stage pipeline illustrated in Figure 3: task curation from existing benchmarks, task design with cross-topology alignment, example generation, and multi-stage quality assurance. Key facts are provided below with comprehensive details in Appendix.

**Task Curation.** We first surveyed prominent visual reasoning benchmarks (e.g., MMMU Pro, MathVista, EMMA [18, 21, 41]) to identify tasks that heavily rely on grid-based spatial logic. Using a combination of LLM-assisted filtering and manual review, we selected tasks whose core reasoning logic can be faithfully re-formulated across different coordinate topologies (Section 3.1).

**Task Design and Cross-Topology Alignment.** For each curated task, we designed paired Cartesian and Polar implementations that preserve equivalent evaluation conditions. This involves three interrelated design considerations. First, *logical alignment*: for each task, we analyzed and designed the wrapping behavior and topological alignment to ensure consistent evaluation across coordinate systems (Section 3.1). Second, *visual calibration*: since the Polar mapping introduces nonlinear distortion, we calibrate the rendering of each task so that size-sensitive visual elements remain as comparable as possible across the two layouts, ensuring that performance differences stem from the coordinate transformation rather than perceptual disadvantage. Third, *narrative design*: beyond adapting existing task formats, we substantially redesigned task rules, visual presentations, and problem structures to introduce richer reasoning demands, and contextualized them within diverse textual scenarios (e.g., robotic navigation, physics simulations).

**Procedural Generation.** Each task is implemented as a self-contained generative script capable of producing unlimited unique instances. We heavily randomize both visual and logical axes (e.g., grid dimensions, starting positions, path topologies, distractors, color palettes), while enforcing

Table 1 | Main results on the Polar benchmark. All models are evaluated under high reasoning mode. C and P denote Cartesian and Polar accuracy (%), respectively. Accuracy score is averaged over the tasks covered. (−Δ) indicates the accuracy drop from Cartesian to Polar. The highest and second-highest scores are highlighted in **bold** and underline, respectively.

| Model                      | Algorithmic Logic & Simulation |                     | Combinatorics & Probability |                     | Navigation & Routing |                     | Spatial Transformation & Geometry |                     | Visual Pattern Matching |                     | Overall     |                     |
|----------------------------|--------------------------------|---------------------|-----------------------------|---------------------|----------------------|---------------------|-----------------------------------|---------------------|-------------------------|---------------------|-------------|---------------------|
|                            | C                              | P (−Δ)              | C                           | P (−Δ)              | C                    | P (−Δ)              | C                                 | P (−Δ)              | C                       | P (−Δ)              | C           | P (−Δ)              |
| Random                     | 17.0                           | 17.0                | 6.7                         | 6.7                 | 18.4                 | 18.4                | 16.2                              | 16.2                | 19.0                    | 19.0                | 15.8        | 15.8                |
| <i>Close Source MLLMs</i>  |                                |                     |                             |                     |                      |                     |                                   |                     |                         |                     |             |                     |
| Gemini-3.1-Pro [16]        | <b>85.0</b>                    | <b>52.6</b> (−32.4) | <b>92.4</b>                 | <b>24.9</b> (−67.6) | <b>83.4</b>          | 39.4 (−44.0)        | <b>83.7</b>                       | <b>31.4</b> (−52.3) | <b>71.0</b>             | <b>36.6</b> (−34.4) | <b>82.6</b> | <b>35.9</b> (−46.7) |
| Gemini-3-Flash [14]        | 68.8                           | 41.5 (−27.3)        | 74.8                        | 20.6 (−54.2)        | 76.2                 | 41.9 (−34.4)        | 68.7                              | 29.8 (−38.8)        | 65.0                    | 34.8 (−30.2)        | 71.0        | 33.8 (−37.2)        |
| Gemini-3-Flash-lite [15]   | 58.0                           | 28.3 (−29.7)        | 40.4                        | 15.9 (−24.6)        | 54.6                 | 28.8 (−25.8)        | 40.6                              | 21.7 (−18.9)        | 43.3                    | 27.7 (−15.5)        | 46.8        | 24.6 (−22.2)        |
| Gemini-2.5-Pro [9]         | 54.3                           | 30.2 (−24.2)        | 23.3                        | 12.7 (−10.7)        | 45.6                 | 31.1 (−14.5)        | 33.8                              | 23.9 (−9.8)         | 38.4                    | 27.0 (−11.4)        | 38.4        | 25.3 (−13.2)        |
| Gemini-2.5-Flash [9]       | 51.3                           | 27.7 (−23.7)        | 15.9                        | 9.4 (−6.4)          | 38.7                 | 26.8 (−11.9)        | 26.4                              | 18.5 (−7.9)         | 33.8                    | 22.7 (−11.1)        | 32.2        | 21.1 (−11.2)        |
| Gpt-5.2 [27]               | <u>70.7</u>                    | <u>46.7</u> (−24.0) | <b>84.8</b>                 | <b>30.7</b> (−54.1) | <b>82.2</b>          | <b>42.8</b> (−39.4) | <b>76.5</b>                       | <b>41.6</b> (−34.9) | <b>70.0</b>             | <b>34.5</b> (−35.5) | <b>77.4</b> | <b>39.2</b> (−38.2) |
| Claude-Sonnet-4.6 [2]      | 60.0                           | 30.3 (−29.7)        | 42.7                        | 16.8 (−25.9)        | 45.0                 | 28.5 (−16.4)        | 42.3                              | 25.2 (−17.0)        | 38.9                    | 28.3 (−10.6)        | 44.4        | 25.9 (−18.5)        |
| Grok-4-0709 [35]           | 53.2                           | 32.8 (−20.4)        | 20.8                        | 12.0 (−8.8)         | 38.0                 | 24.9 (−13.1)        | 29.9                              | 22.2 (−7.7)         | 29.5                    | 19.6 (−9.9)         | 33.0        | 21.8 (−11.2)        |
| Grok-4-Fast-Reasoning [35] | 49.7                           | 30.8 (−18.8)        | 17.7                        | 12.3 (−5.3)         | 37.7                 | 27.1 (−10.6)        | 28.4                              | 21.5 (−6.8)         | 26.1                    | 20.5 (−5.5)         | 31.0        | 22.3 (−8.7)         |
| <i>Open Source MLLMs</i>   |                                |                     |                             |                     |                      |                     |                                   |                     |                         |                     |             |                     |
| Qwen3.5-397B-A17B [24]     | <u>72.2</u>                    | <b>43.2</b> (−29.0) | <u>65.2</u>                 | <u>18.1</u> (−47.1) | <b>77.6</b>          | <b>40.9</b> (−36.7) | <b>77.2</b>                       | <b>39.5</b> (−37.8) | <b>68.5</b>             | <b>31.5</b> (−37.0) | <b>72.9</b> | <b>35.0</b> (−37.9) |
| Kimi-k2.5 [29]             | <b>73.5</b>                    | <b>37.3</b> (−36.1) | <b>68.7</b>                 | 16.2 (−52.5)        | <b>73.0</b>          | <b>38.3</b> (−34.7) | <b>71.7</b>                       | <b>31.1</b> (−40.6) | <b>58.4</b>             | <b>30.8</b> (−27.5) | <b>69.0</b> | <b>31.1</b> (−37.8) |
| Gemma-4-31B [10]           | 67.7                           | 36.0 (−31.7)        | 62.3                        | <b>19.4</b> (−42.8) | 63.9                 | 37.6 (−26.2)        | 60.1                              | 28.5 (−31.6)        | 51.5                    | <b>32.5</b> (−19.1) | <b>60.5</b> | 31.0 (−29.5)        |
| Gemma-4-26B [10]           | 56.0                           | 29.5 (−26.5)        | 45.8                        | 14.8 (−30.9)        | 48.9                 | 26.5 (−22.4)        | 48.5                              | 19.4 (−29.2)        | 40.0                    | 25.4 (−14.6)        | 47.2        | 22.9 (−24.4)        |
| Mistral-Small-2503 [1]     | 25.0                           | 20.7 (−4.4)         | 9.6                         | 10.9 (1.3)          | 22.6                 | 21.2 (−1.4)         | 19.5                              | 21.2 (1.7)          | 20.3                    | 19.4 (−0.9)         | 19.4        | 19.0 (−0.4)         |

programmatic solvability checks to prevent degenerate configurations. Each task contributes 100 paired Cartesian–Polar instances to the final benchmark.

#### Quality Assurance and Human Validation.

We implement a multi-stage verification pipeline to ensure the correctness and clarity of generated data. (1) We iteratively refined the rendering to ensure visual clarity and legibility across both Cartesian and Polar layouts. (2) The authors verified task logic through collaborative review and by independently spot-checking and solving sampled instances across all 53 tasks. (3) We employed LLM-assisted audits of the procedural code to identify unhandled edge cases. Steps (1)–(3) were repeated until no further issues were identified. (4) As a final safeguard, we conducted a human validation study in which independent raters manually solved 20 randomly sampled Cartesian–Polar pairs per task, confirming the correctness and quality of the final benchmark data.

## 4. Experiments

### 4.1. Experimental setup

#### Evaluated Models.

To comprehensively evaluate visual reasoning capabilities, we test a diverse suite of state-of-the-art Multimodal Large Language Models spanning both proprietary and open-source families. For proprietary models, we include the Gemini family (*Gemini-3.1-Pro*, *Gemini-3-Flash*, *Gemini-3.1-Flash-Lite*, *Gemini-2.5-Pro*, *Gemini-2.5-Flash*) [9, 14–16], *GPT-5.2* [27], *Claude-Sonnet-4.6* [2], and *Grok-4* family (*Grok-4-0709*, *Grok-4-Fast-Reasoning*, *Grok-4-Fast-Non-Reasoning*) [35]. For open-source models, we evaluate *Gemma-4-31B*, *Gemma-4-26B* [10], *Kimi-k2.5* [29], *Qwen-3.5-397B-A17B* [24], and *Mistral-Small-3.1-24B* [1]. This diverse model selection spans different architectures, scales, and training recipes, and allows us to assess whether the Cartesian Shortcut is a universal limitation or an artifact of specific model families. All models are accessed via public APIs with default parameter settings and maximum supported context length.

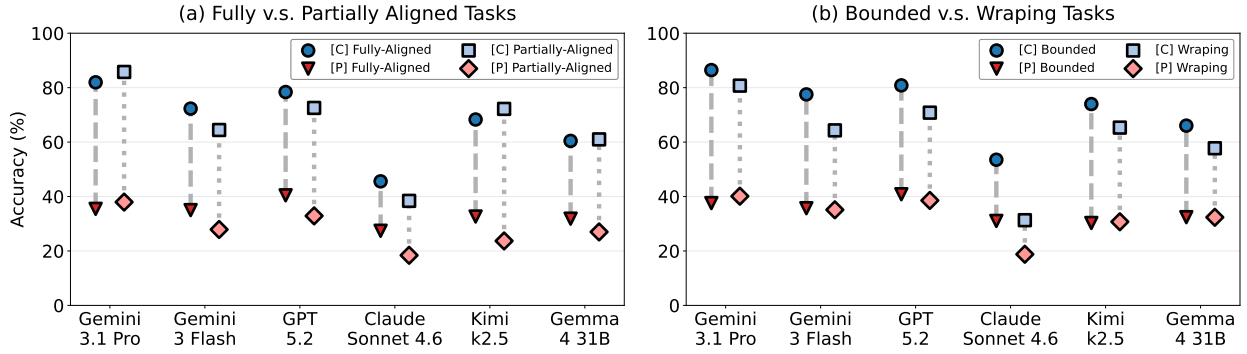


Figure 5 | Cartesian and Polar accuracy under different topological alignment conditions. (a) Fully aligned vs. partially aligned tasks. Both subsets exhibit comparable Cartesian-to-Polar drops across all models. (b) Bounded vs. wrapping tasks. Both conditions exhibit consistent Cartesian-to-Polar drops, with wrapping tasks showing slightly lower overall accuracy.

**Reasoning Modes.** For the subset of models supporting configurable reasoning, we evaluate under two inference settings: (1) a *high reasoning* mode that activates the model’s highest supported Chain-of-Thought setting; and (2) a *non-reasoning* mode that uses the minimal reasoning configuration.

**Evaluation Metrics.** Since ground-truth answers in Polaris-Bench are deterministic and span well-defined formats (option labels, digits, coordinate positions, strings and lists), we employ exact-match accuracy as our primary metric. For the small fraction of responses whose format deviates from the expected structure, we apply LLM-as-a-judge (i.e., Gemini-3.1-Pro) as a calibration fallback to ensure fair evaluation [17, 43]. We additionally report a theoretical random baseline computed from the statistical expectation of each task’s answer format as a lower-bound reference. All models and tasks share the same prompt templates, provided in Appendix.

## 4.2. Main results

The main results in Table 1 report overall and per-category accuracy for all evaluated models under high reasoning mode, comparing Cartesian (C) and Polar (P) layouts. Figure 5 examines topological alignment conditions. Table 2 reports reasoning vs. non-reasoning inference for configurable models. Figure 6 visualize the comparison in Table 1,2. Figure 7(a) provides a representative failure case.

**All models exhibit a consistent performance collapse on Polar layouts.** Table 1 and Figure 6(a) present the Cartesian and Polar accuracy across all evaluated models. Frontier models achieving 70–83% on Cartesian layouts collapse to 31–39% on Polar equivalents, with the largest drop over 45 points. Notably, while Cartesian accuracy varies widely across model families (e.g., 82.6% for Gemini-3.1-Pro, 33.0% for Grok-4-0709), Polar scores compress into a narrow band, suggesting a shared performance floor dictated by the absence of topology-invariant reasoning rather than model-specific capacity. Per-category analysis reveals that this collapse is non-uniform: *Combinatorics & Probability* suffers the steepest degradation (e.g., 92.4  $\rightarrow$  24.9 for Gemini-3.1-Pro, 68.7  $\rightarrow$  16.2 for Kimi-k2.5), which we hypothesize relates to the tasks’ deeper dependency on structured grid enumeration. *Algorithmic Logic & Simulation* retains comparatively higher Polar accuracy (e.g., 52.6% for Gemini-3.1-Pro). All models fall well below the ideal topological invariance line (Figure 6(a)); this consistency across diverse model families, scales, and training paradigms confirms that the Cartesian Shortcut constitutes a systemic vulnerability rather than a model-specific limitation.

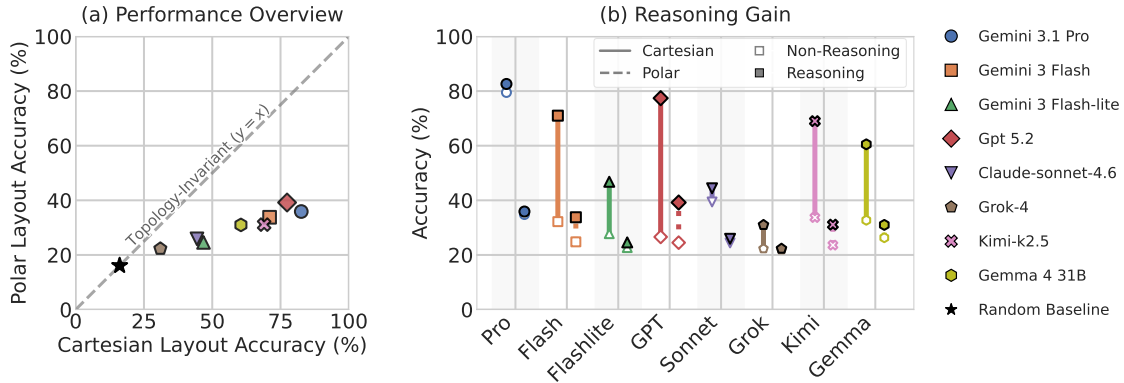


Figure 6 | Performance overview and reasoning mode effect. (a) Overall Cartesian vs. Polar accuracy for each model (reasoning: high). (b) Reasoning effect on Cartesian and Polar accuracy. Connected pairs show the reasoning gains on Cartesian layouts consistently diminish on Polar equivalents.

**Performance collapse persists across topological alignment conditions.** Figure 5 examines whether the collapse is attributable to the coordinate transformation itself or to confounds introduced by altered solution spaces or boundary conditions (Section 3). On *fully aligned* tasks (Figure 5(a)), where the coordinate transformation is the sole variable, all models still exhibit severe collapse (e.g., Gemini-3.1-Pro: 82.0  $\rightarrow$  35.5, Kimi-k2.5: 68.3  $\rightarrow$  32.6) comparable in magnitude to the overall and partially aligned results. This provides direct evidence that coordinate transformation alone suffices to disrupt model performance. *Partially aligned* tasks show marginally larger gaps (e.g., Gemini-3.1-Pro: 85.8  $\rightarrow$  38.0), yet the collapse trend remains consistent. The *bounded vs. wrapping* comparison (Figure 5(b)) similarly reveals no substantial divergence across all evaluated models. Together, these results confirm that the performance collapse is predominantly driven by the topology transformation itself, with specific topological configurations exerting limited additional influence.

**Reasoning gains on Cartesian layouts are severely diminished on Polar equivalents.** Table 2 and Figure 6(b) compare model performance under high reasoning and non-reasoning modes. On Cartesian layouts, enabling reasoning yields substantial accuracy improvements, with gains up to 50.8 points (GPT-5.2) and several models exceeding 30 points. However, on Polar layouts these gains are systematically compressed, with most models improving by fewer than 10 points: Gemini-3-Flash’s gain shrinks from 38.7 to 9.0, Kimi-k2.5 from 35.2 to 7.6. At the category level, this pattern mirrors the findings in Table 1: *Combinatorics & Probability*, which benefits more from reasoning on Cartesian (e.g., Gemini-3-Flash: 60.6 points), sees these gains collapse more severely on Polar (8.9 points), while *Algorithmic Logic & Simulation* retains comparatively more of its reasoning benefit. This asymmetry reveals a strong correlation between reasoning effectiveness and the availability of the Cartesian Shortcut: reasoning substantially amplifies performance when the orthogonal prior exists, but this amplification diminishes correspondingly once shortcut is disrupted by Polar transformation.

## 5. Discussions

**Effect of out-of-distribution (OOD).** Polar layouts are inherently less prevalent than Cartesian grids in natural training data, raising the question of whether the observed performance collapse is primarily an OOD artifact. To investigate, we conduct two prompting interventions on randomly selected tasks with large performance drops: (1) a *conversion hint* instructing the model to re-map the Polar layout into a Cartesian grid before solving, and (2) *5-shot in-context learning* [11, 23] with solved

Table 2 | Model performance across categories, comparing reasoning modes. ( $-\Delta$ ) are shown alongside the Polar column scores. The third row for each model represents the reasoning gain.

| Model               | Reason | Algorithmic Logic & Simulation |      |                 | Combinatorics & Probability |      |                 | Navigation & Routing |      |                 | Spatial Transformation & Geometry |      |                 | Visual Pattern Matching |      |                 | Overall |      |         |
|---------------------|--------|--------------------------------|------|-----------------|-----------------------------|------|-----------------|----------------------|------|-----------------|-----------------------------------|------|-----------------|-------------------------|------|-----------------|---------|------|---------|
|                     |        | C                              | P    | P ( $-\Delta$ ) | C                           | P    | P ( $-\Delta$ ) | C                    | P    | P ( $-\Delta$ ) | C                                 | P    | P ( $-\Delta$ ) | C                       | P    | P ( $-\Delta$ ) |         |      |         |
| Gemini-3.1-Pro      | ✓      | 85.0                           | 52.6 | (-32.4)         | 92.4                        | 24.9 | (-67.6)         | 83.4                 | 39.4 | (-44.0)         | 83.7                              | 31.4 | (-52.3)         | 71.0                    | 36.6 | (-34.4)         | 82.6    | 35.9 | (-46.7) |
|                     | ×      | 66.7                           | 35.6 | (-31.1)         | 83.4                        | 22.7 | (-60.7)         | 82.9                 | 42.6 | (-40.3)         | 86.2                              | 31.8 | (-54.4)         | 71.3                    | 37.6 | (-33.7)         | 79.5    | 34.8 | (-44.8) |
|                     |        | 18.3                           | 16.9 |                 | 9.1                         | 2.2  |                 | 0.5                  | -3.2 |                 | -2.5                              | -0.4 |                 | -0.3                    | -1.0 |                 | 3.1     | 1.1  |         |
| Gemini-3-Flash      | ✓      | 68.8                           | 41.5 | (-27.3)         | 74.8                        | 20.6 | (-54.2)         | 76.2                 | 41.9 | (-34.4)         | 68.7                              | 29.8 | (-38.8)         | 65.0                    | 34.8 | (-30.2)         | 71.0    | 33.8 | (-37.2) |
|                     | ×      | 34.2                           | 19.3 | (-14.8)         | 14.2                        | 11.7 | (-2.6)          | 42.9                 | 37.1 | (-5.9)          | 28.5                              | 24.1 | (-4.5)          | 36.7                    | 24.0 | (-12.7)         | 32.2    | 24.8 | (-7.4)  |
|                     |        | 34.7                           | 22.2 |                 | 60.6                        | 8.9  |                 | 33.3                 | 4.8  |                 | 40.2                              | 5.8  |                 | 28.3                    | 10.8 |                 | 38.7    | 9.0  |         |
| Gemini-3-Flash-lite | ✓      | 58.0                           | 28.3 | (-29.7)         | 40.4                        | 15.9 | (-24.6)         | 54.6                 | 28.8 | (-25.8)         | 40.6                              | 21.7 | (-18.9)         | 43.3                    | 27.7 | (-15.5)         | 46.8    | 24.6 | (-22.2) |
|                     | ×      | 26.5                           | 19.2 | (-7.3)          | 9.9                         | 9.3  | (-0.6)          | 36.7                 | 33.0 | (-3.7)          | 23.7                              | 19.3 | (-4.4)          | 36.7                    | 26.5 | (-10.3)         | 27.8    | 22.7 | (-5.1)  |
|                     |        | 31.5                           | 9.2  |                 | 30.6                        | 6.6  |                 | 17.9                 | -4.2 |                 | 16.9                              | 2.4  |                 | 6.5                     | 1.3  |                 | 19.0    | 1.9  |         |
| GPT-5.2             | ✓      | 70.7                           | 46.7 | (-24.0)         | 84.8                        | 30.7 | (-54.1)         | 82.2                 | 42.8 | (-39.4)         | 76.5                              | 41.6 | (-34.9)         | 70.0                    | 34.5 | (-35.5)         | 77.4    | 39.2 | (-38.2) |
|                     | ×      | 32.9                           | 28.0 | (-5.0)          | 11.2                        | 10.7 | (-0.5)          | 29.3                 | 28.6 | (-0.8)          | 24.1                              | 25.2 | (1.1)           | 35.4                    | 28.1 | (-7.3)          | 26.6    | 24.5 | (-2.1)  |
|                     |        | 37.8                           | 18.7 |                 | 73.6                        | 20.0 |                 | 52.8                 | 14.2 |                 | 52.4                              | 16.5 |                 | 34.6                    | 6.4  |                 | 50.8    | 14.6 |         |
| Claude-Sonnet-4.6   | ✓      | 60.0                           | 30.3 | (-29.7)         | 42.7                        | 16.8 | (-25.9)         | 45.0                 | 28.5 | (-16.4)         | 42.3                              | 25.2 | (-17.0)         | 38.9                    | 28.3 | (-10.6)         | 44.4    | 25.9 | (-18.5) |
|                     | ×      | 45.4                           | 26.9 | (-18.5)         | 42.6                        | 16.7 | (-25.9)         | 45.5                 | 25.5 | (-20.0)         | 29.6                              | 24.0 | (-5.6)          | 37.5                    | 28.4 | (-9.1)          | 39.4    | 24.4 | (-15.0) |
|                     |        | 14.6                           | 3.4  |                 | 0.2                         | 0.2  |                 | -0.5                 | 3.0  |                 | 12.6                              | 1.2  |                 | 1.5                     | -0.0 |                 | 4.9     | 1.5  |         |
| Grok-4              | ✓      | 49.7                           | 30.8 | (-18.8)         | 17.7                        | 12.3 | (-5.3)          | 37.7                 | 27.1 | (-10.6)         | 28.4                              | 21.5 | (-6.8)          | 26.1                    | 20.5 | (-5.5)          | 31.0    | 22.3 | (-8.7)  |
|                     | ×      | 18.2                           | 17.8 | (-0.4)          | 10.5                        | 10.7 | (0.2)           | 35.3                 | 36.8 | (1.5)           | 19.1                              | 18.9 | (-0.3)          | 21.5                    | 18.1 | (-3.4)          | 22.3    | 21.9 | (-0.4)  |
|                     |        | 31.5                           | 13.0 |                 | 7.1                         | 1.6  |                 | 2.4                  | -9.7 |                 | 9.2                               | 2.7  |                 | 4.6                     | 2.4  |                 | 8.6     | 0.3  |         |
| Kimi-k2.5           | ✓      | 73.5                           | 37.3 | (-36.1)         | 68.7                        | 16.2 | (-52.5)         | 73.0                 | 38.3 | (-34.7)         | 71.7                              | 31.1 | (-40.6)         | 58.4                    | 30.8 | (-27.5)         | 69.0    | 31.1 | (-37.8) |
|                     | ×      | 44.5                           | 25.4 | (-19.1)         | 20.9                        | 8.0  | (-12.9)         | 37.2                 | 29.9 | (-7.4)          | 27.8                              | 23.2 | (-4.6)          | 40.9                    | 27.7 | (-13.2)         | 33.7    | 23.6 | (-10.2) |
|                     |        | 29.0                           | 12.0 |                 | 47.8                        | 8.2  |                 | 35.7                 | 8.4  |                 | 43.9                              | 8.0  |                 | 17.5                    | 3.1  |                 | 35.2    | 7.6  |         |
| Gemma-4-31B         | ✓      | 67.7                           | 36.0 | (-31.7)         | 62.3                        | 19.4 | (-42.8)         | 63.9                 | 37.6 | (-26.2)         | 60.1                              | 28.5 | (-31.6)         | 51.5                    | 32.5 | (-19.1)         | 60.5    | 31.0 | (-29.5) |
|                     | ×      | 32.5                           | 21.8 | (-10.7)         | 19.3                        | 11.3 | (-8.0)          | 44.8                 | 38.1 | (-6.7)          | 24.2                              | 22.2 | (-2.0)          | 38.2                    | 30.9 | (-7.3)          | 32.7    | 26.3 | (-6.3)  |
|                     |        | 35.2                           | 14.2 |                 | 42.9                        | 8.1  |                 | 19.1                 | -0.4 |                 | 35.8                              | 6.2  |                 | 13.4                    | 1.5  |                 | 27.9    | 4.7  |         |

Polar examples. As Figure 7(d) shown, accuracy under both interventions remains comparable to the Polar baseline despite per-task fluctuations. While these prompting-level probes do not fully exclude distributional factors, they reveal that the Cartesian Shortcut is not a shallow reasoning heuristic that can be overridden by instruction: even when explicitly guided to convert Polar layouts back to Cartesian grids, models fail to execute this re-mapping, indicating that dependence on orthogonal structure is deeply embedded in how models process and reason over visual information.

**Two boundary tasks exhibit near topological invariance.** We identify two contrasting tasks where models exhibit comparable performance across Cartesian and Polar layouts (Figure 7(b)). In *Maze* task, most models score below 40% on both topologies; in *Monotonic Path* task, leading models exceed 80% on both. Inspection of thinking traces on Monotonic Path reveals that models consistently reference the numerical labels in cells during reasoning (e.g., “currently at 35, move to 45”). In contrast, maze contains no such textual anchors. This suggests that when symbolic anchors are present, models adopt a reasoning strategy functionally analogous to the Cartesian Shortcut, maintaining strong performance regardless of topology. When neither form of textual shortcut is available, Cartesian or task-intrinsic symbolic anchors, models fail uniformly across both layouts.

**The orthogonal discretization vulnerability generalizes beyond Polar.** While Polar serves as our primary diagnostic probe, the topological vulnerability it exposes is not unique to Polar space. To verify, we construct additional layout variants (Octagonal, Hexagonal) for the *Word Search* task tilings alongside a graph-based Polar layout for which a direct Polar grid analog is unavailable (Figure 7(c)). As shown in Figure 7(e), a bimodal pattern emerges: Octagonal grids, which preserve local orthogonal adjacency, maintain near-Cartesian accuracy with modest drop; both Hexagonal and Polar variants

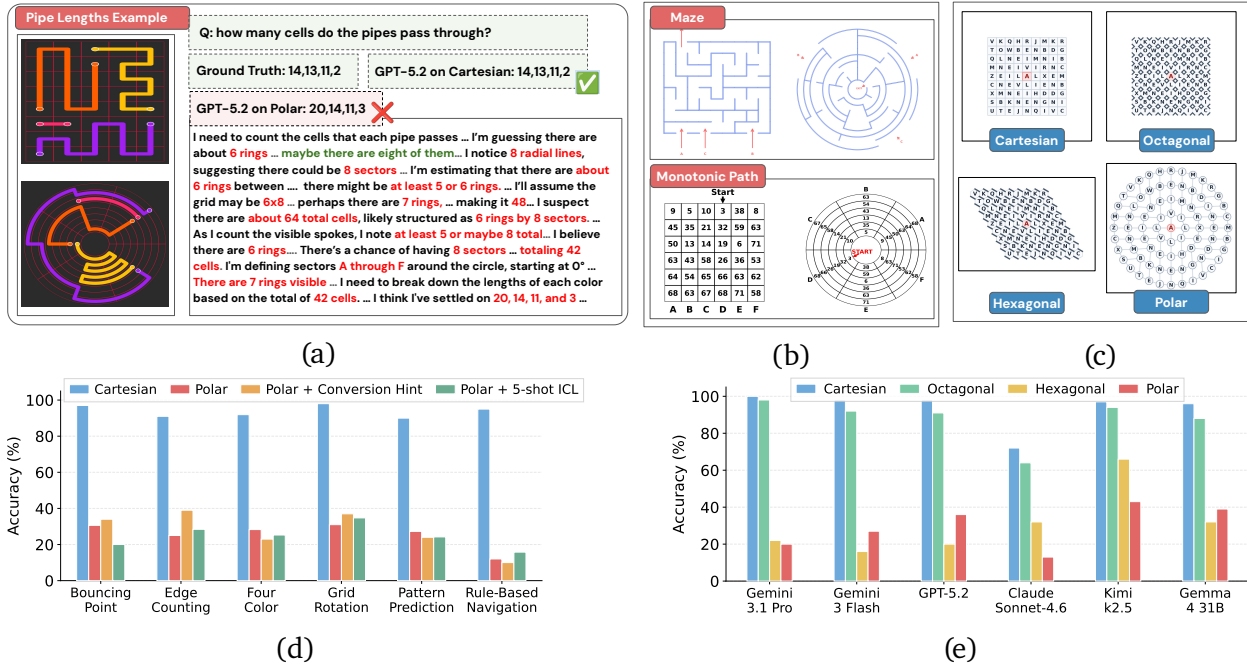


Figure 7 | Qualitative and quantitative analyses for the discussion. (a) Case study on the Pipe Lengths task showing the model fails on Polar with back-and-forth chain-of-thought, revealing persistent confusion over ring and sector indexing. (b) Examples from Maze and Monotonic Path tasks, the two boundary tasks exhibiting near topological invariance. (c) Examples from Word Search task across Cartesian, graph-based Polar and extended Octagonal, Hexagonal layouts. (d) Out-of-distribution analysis on Gemini 3.1 Pro. Per-task accuracy across Cartesian, Polar, Polar with conversion hints, and Polar with 5-shot ICL, showing that scaffolding alone cannot close the gap for visually grounded tasks. (e) Accuracy on 4 layouts of Word Search task evaluated with Gemini 3.1 Pro, confirming that the modality gap extends beyond the Cartesian-Polar dichotomy.

trigger severe collapse. These results demonstrate that different forms of disruption to orthogonal structure degrade model performance to varying degrees; layouts deviating further from the standard grid tend to exhibit more pronounced collapse. This indicates that the lack of topology-invariant visual reasoning is a general phenomenon, not confined to the Cartesian-Polar dichotomy.

**Limitation.** While developing topology-invariant vision reasoning is critical for robust and generalizable multimodal intelligence, we acknowledge that the Cartesian Shortcut reflects genuinely powerful deductive capabilities. In real-world applications where grid-based layouts are ubiquitous, the ability to discretize and reason over orthogonal structures is highly effective. Second, the current scope of Polaris-Bench focuses on 2D visual scenario, extending to 3D spatial structures and broader visual domains remains a future direction. Finally, this work focuses on evaluation and diagnosis of the topological vulnerability. How to improve topology-invariant visual reasoning in MLLMs remains an open and important problem for future research.

## 6. Related works

**Vision reasoning in MLLMs.** The rapid advancement of MLLMs [2, 16, 24, 27, 29] has driven a proliferation of visual reasoning benchmarks evaluating mathematical reasoning [18, 21], multi-discipline understanding [40, 41], spatial reasoning [19], and broader, deeper vision reasoning [6,

22, 30, 32, 33, 37, 44], with several adopting structured grid-based layouts for precise assessment of spatial and algorithmic problem-solving [25, 28]. Alongside this progress, growing evidence questions whether current models genuinely reason over visual content. One line of work reveals that MLLMs fail at perceptual tasks humans find trivial [8, 12, 26, 31, 39]. Another line questions whether strong benchmark scores genuinely reflect visual understanding [4, 7, 38]: evaluation practices may overestimate true capability [7], reasoning modes can amplify hallucination rather than improve visual grounding [38], and frontier models generate elaborate reasoning for images never provided [4]. These concerns connect to shortcut learning [13, 36]: models exploiting superficial regularities that generalize within benchmarks but collapse under distribution shift. However, the specific mechanism by which models circumvent genuine visual reasoning remains unidentified. In this work, we identify and empirically validate the pervasively exist Cartesian Shortcut: models leverage the orthogonal structure of grid-based layouts to offload visual reasoning onto text-based deduction.

**Coordinate systems and geometric foundations.** Standard neural architectures are built upon grid-structured representations with inherent translational symmetry [5], an architectural prior that may contribute to model’s Cartesian deduction behavior. The equivalence and duality between different coordinate representations has long been studied in mathematics [3] and vision science [42]. To our knowledge, this is the first work to leverage coordinate transformation as a systematic diagnostic probe for visual reasoning evaluation in MLLMs.

## 7. Conclusion

In this work, we identify and empirically validate the Cartesian Shortcut, a pervasive vulnerability whereby MLLMs systematically discretize orthogonal grid layouts into textual coordinates, offloading visual reasoning onto text-based deduction. We introduce Polaris-Bench, a controlled diagnostic benchmark of 53 paired Cartesian–Polar visual reasoning tasks, and demonstrate a universal performance collapse when the orthogonal structure is disrupted, with degradation persisting even under complete logical equivalence and reasoning gains severely diminished on Polar equivalents. These findings, consistent across diverse model families, scales, and layout geometries, establish that current MLLMs fundamentally lack topology-invariant visual reasoning capability. Developing visual reasoning that generalizes reliably across diverse topological structures is essential for truly robust multimodal intelligence, and that their abilities may be systematically overestimated on grid-based layouts. Ultimately, we hope this work motivates future research toward genuine layout-agnostic visual reasoning.

## References

- [1] M. AI. Mistral-small-3.1-24b-instruct-2503, March 2025. URL <https://mistral.ai/news/mistral-small-3-1>.
- [2] A. Anthropic. The claude 3 model family: Opus, sonnet, haiku. *Claude-3 Model Card*, 1(1):4, 2024.
- [3] G. B. Arfken, H. J. Weber, and F. E. Harris. *Mathematical methods for physicists: a comprehensive guide*. Academic press, 2011.
- [4] M. Asadi, J. W. O’Sullivan, F. Cao, T. Nedaei, K. Rajabalifardi, F.-F. Li, E. Adeli, and E. Ashley. Mirage: The illusion of visual understanding, 2026. URL <https://arxiv.org/abs/2603.21687>.

- 
- [5] M. M. Bronstein, J. Bruna, T. Cohen, and P. Veličković. Geometric deep learning: Grids, groups, graphs, geodesics, and gauges. *arXiv preprint arXiv:2104.13478*, 2021.
- [6] J. Chen, T. Liang, S. Siu, Z. Wang, K. Wang, Y. Wang, Y. Ni, W. Zhu, Z. Jiang, B. Lyu, D. Jiang, X. He, Y. Liu, H. Hu, X. Yue, and W. Chen. Mega-bench: Scaling multimodal evaluation to over 500 real-world tasks. 2025.
- [7] L. Chen, J. Li, X. Dong, P. Zhang, Y. Zang, Z. Chen, H. Duan, J. Wang, Y. Qiao, D. Lin, et al. Are we on the right way for evaluating large vision-language models? *Advances in Neural Information Processing Systems*, 37:27056–27087, 2024.
- [8] L. Chen, W. Xie, Y. Liang, H. He, H. Zhao, Z. Yang, Z. Huang, H. Wu, H. Lu, Y. Charles, Y. Bao, Y. Fan, G. Li, H. Shen, X. Chen, W. Xu, S. Si, Z. Cai, W. Chai, Z. Huang, F. Liu, T. Liu, B. Chang, X. Hu, K. Chen, Y. Ren, Y. Liu, Y. Gong, and K. Li. Babyvision: Visual reasoning beyond language, 2026. URL <https://arxiv.org/abs/2601.06521>.
- [9] G. Comanici, E. Bieber, M. Schaekermann, I. Pasupat, N. Sachdeva, I. Dhillon, M. Blistein, O. Ram, D. Zhang, E. Rosen, et al. Gemini 2.5: Pushing the frontier with advanced reasoning, multimodality, long context, and next generation agentic capabilities. *arXiv preprint arXiv:2507.06261*, 2025.
- [10] G. DeepMind. Gemma 4: Our most intelligent open models to date. <https://blog.google/innovation-and-ai/technology/developers-tools/gemma-4/>, 2026. Accessed: 2026-05-01.
- [11] Q. Dong, L. Li, D. Dai, C. Zheng, J. Ma, R. Li, H. Xia, J. Xu, Z. Wu, T. Liu, B. Chang, X. Sun, L. Li, and Z. Sui. A survey on in-context learning, 2024. URL <https://arxiv.org/abs/2301.00234>.
- [12] X. Fu, Y. Hu, B. Li, Y. Feng, H. Wang, X. Lin, D. Roth, N. A. Smith, W.-C. Ma, and R. Krishna. Blink: Multimodal large language models can see but not perceive. *arXiv preprint arXiv:2404.12390*, 2024.
- [13] R. Geirhos, J.-H. Jacobsen, C. Michaelis, R. Zemel, W. Brendel, M. Bethge, and F. A. Wichmann. Shortcut learning in deep neural networks. *Nature Machine Intelligence*, 2(11):665–673, 2020.
- [14] Gemini Team and Google DeepMind. Gemini 3 flash: Frontier intelligence built for speed. Technical blog / model release, Google, 12 2025. URL <https://blog.google/products-and-platforms/products/gemini/gemini-3-flash/>.
- [15] Gemini Team and Google DeepMind. Gemini 3.1 flash-lite: Built for intelligence at scale. Technical blog / model release, Google, 3 2026. URL <https://blog.google/innovation-and-ai/models-and-research/gemini-models/gemini-3-1-flash-lite/>.
- [16] Gemini Team, Google. Gemini 3 pro technical report. 2025. URL <https://deepmind.google/models/gemini/pro/>.
- [17] J. Gu, X. Jiang, Z. Shi, H. Tan, X. Zhai, C. Xu, W. Li, Y. Shen, S. Ma, H. Liu, et al. A survey on llm-as-a-judge. *The Innovation*, 2024.
- [18] Y. Hao, J. Gu, H. W. Wang, L. Li, Z. Yang, L. Wang, and Y. Cheng. Can MLLMs reason in multimodality? EMMA: An enhanced multimodal reasoning benchmark. In *Forty-second International Conference on Machine Learning*, 2025. URL <https://openreview.net/forum?id=v26vwjx0Ez>.
-

- [19] M. Jia, Z. Qi, S. Zhang, W. Zhang, X. Yu, J. He, H. Wang, and L. Yi. Omnispatial: Towards comprehensive spatial reasoning benchmark for vision language models. In *The Fourteenth International Conference on Learning Representations*, 2026. URL <https://openreview.net/forum?id=6nZKT2rL0H>.
- [20] A. S. Kanade and T. Ganu. Do you see me : A multidimensional benchmark for evaluating visual perception in multimodal LLMs. In V. Demberg, K. Inui, and L. Marquez, editors, *Proceedings of the 19th Conference of the European Chapter of the Association for Computational Linguistics (Volume 1: Long Papers)*, pages 7285–7326, Rabat, Morocco, Mar. 2026. Association for Computational Linguistics. ISBN 979-8-89176-380-7. doi: 10.18653/v1/2026.eacl-long.343. URL <https://aclanthology.org/2026.eacl-long.343/>.
- [21] P. Lu, H. Bansal, T. Xia, J. Liu, C. Li, H. Hajishirzi, H. Cheng, K.-W. Chang, M. Galley, and J. Gao. Mathvista: Evaluating mathematical reasoning of foundation models in visual contexts. In *The Twelfth International Conference on Learning Representations*, 2024.
- [22] F. Meng, J. Wang, C. Li, Q. Lu, H. Tian, J. Liao, X. Zhu, J. Dai, Y. Qiao, P. Luo, K. Zhang, and W. Shao. Mmiu: Multimodal multi-image understanding for evaluating large vision-language models, 2024. URL <https://arxiv.org/abs/2408.02718>.
- [23] S. Min, X. Lyu, A. Holtzman, M. Artetxe, M. Lewis, H. Hajishirzi, and L. Zettlemoyer. Rethinking the role of demonstrations: What makes in-context learning work? In *Proceedings of the 2022 conference on empirical methods in natural language processing*, pages 11048–11064, 2022.
- [24] Qwen Team. Qwen3.5: Towards native multimodal agents, February 2026. URL <https://qwen.ai/blog?id=qwen3.5>.
- [25] Y. Ren, K. Tertikas, S. Maiti, J. Han, T. Zhang, S. Ssstrunk, and F. Kokkinos. Vgrp-bench: Visual grid reasoning puzzle benchmark for large vision-language models. *arXiv preprint arXiv:2503.23064*, 2025.
- [26] R. Saxena, A. P. Gema, and P. Minervini. Lost in time: Clock and calendar understanding challenges in multimodal llms, 2025. URL <https://arxiv.org/abs/2502.05092>.
- [27] A. Singh, A. Fry, A. Perelman, A. Tart, A. Ganesh, A. El-Kishky, A. McLaughlin, A. Low, A. Ostrow, A. Ananthram, et al. Openai gpt-5 system card. *arXiv preprint arXiv:2601.03267*, 2025.
- [28] Z. Tang and M. Kejriwal. Grasp: A grid-based benchmark for evaluating commonsense spatial reasoning, 2025. URL <https://arxiv.org/abs/2407.01892>.
- [29] K. Team, T. Bai, Y. Bai, Y. Bao, S. Cai, Y. Cao, Y. Charles, H. Che, C. Chen, G. Chen, et al. Kimi k2. 5: Visual agentic intelligence. *arXiv preprint arXiv:2602.02276*, 2026.
- [30] S. Tong, E. L. B. II, P. Wu, S. Woo, A. J. IYER, S. C. Akula, S. Yang, J. Yang, M. Middepogu, Z. Wang, X. Pan, R. Fergus, Y. LeCun, and S. Xie. Cambrian-1: A fully open, vision-centric exploration of multimodal LLMs. In *The Thirty-eighth Annual Conference on Neural Information Processing Systems*, 2024. URL <https://openreview.net/forum?id=Vi8AepAXGy>.
- [31] S. Tong, Z. Liu, Y. Zhai, Y. Ma, Y. LeCun, and S. Xie. Eyes wide shut? exploring the visual shortcomings of multimodal llms. In *Proceedings of the IEEE/CVF conference on computer vision and pattern recognition*, pages 9568–9578, 2024.
- [32] F. Wang, X. Fu, J. Y. Huang, Z. Li, Q. Liu, X. Liu, M. D. Ma, N. Xu, W. Zhou, K. Zhang, et al. Muirbench: A comprehensive benchmark for robust multi-image understanding. *arXiv preprint arXiv:2406.09411*, 2024.

- [33] Z. Wang, M. Xia, L. He, H. Chen, Y. Liu, R. Zhu, K. Liang, X. Wu, H. Liu, S. Malladi, A. Chevalier, S. Arora, and D. Chen. Charxiv: Charting gaps in realistic chart understanding in multimodal llms. *arXiv preprint arXiv:2406.18521*, 2024.
- [34] J. Wei, X. Wang, D. Schuurmans, M. Bosma, F. Xia, E. Chi, Q. V. Le, D. Zhou, et al. Chain-of-thought prompting elicits reasoning in large language models. *Advances in neural information processing systems*, 35:24824–24837, 2022.
- [35] xAI. Grok-4 model card. 2025. URL <https://x.ai/news/grok-4>.
- [36] J. Xia, Y. Zang, P. Gao, S. Li, and K. Zhou. Visionary-r1: Mitigating shortcuts in visual reasoning with reinforcement learning, 2025. URL <https://arxiv.org/abs/2505.14677>.
- [37] W. Xu, J. Wang, W. Wang, Z. Chen, W. Zhou, A. Yang, L. Lu, H. Li, X. Wang, X. Zhu, W. Wang, J. Dai, and J. Zhu. Visulogic: A benchmark for evaluating visual reasoning in multi-modal large language models. *arXiv preprint arXiv:2504.15279*, 2025. URL <https://arxiv.org/abs/2504.15279>.
- [38] Z. Xu, C. Liu, Q. Wei, J. Wu, J. Zou, X. E. Wang, Y. Zhou, and S. Liu. More thinking, less seeing? assessing amplified hallucination in multimodal reasoning models. In *The Thirty-ninth Annual Conference on Neural Information Processing Systems*, 2025.
- [39] J. Ye, D. Jiang, J. He, B. Zhou, Z. Huang, Z. Yan, H. Li, C. He, and W. Li. BLINK-twice: You see, but do you observe? a reasoning benchmark on visual perception. In *The Thirty-ninth Annual Conference on Neural Information Processing Systems Datasets and Benchmarks Track*, 2026. URL <https://openreview.net/forum?id=g0AMmWiHCq>.
- [40] X. Yue, Y. Ni, K. Zhang, T. Zheng, R. Liu, G. Zhang, S. Stevens, D. Jiang, W. Ren, Y. Sun, et al. Mmmu: A massive multi-discipline multimodal understanding and reasoning benchmark for expert agi. In *Proceedings of the IEEE/CVF conference on computer vision and pattern recognition*, pages 9556–9567, 2024.
- [41] X. Yue, T. Zheng, Y. Ni, Y. Wang, K. Zhang, S. Tong, Y. Sun, B. Yu, G. Zhang, H. Sun, et al. Mmmu-pro: A more robust multi-discipline multimodal understanding benchmark. In *Proceedings of the 63rd Annual Meeting of the Association for Computational Linguistics (Volume 1: Long Papers)*, pages 15134–15186, 2025.
- [42] C. Zetsche, G. Krieger, and B. Wegmann. The atoms of vision: Cartesian or polar? *Journal of the Optical Society of America A*, 16(7):1554–1565, 1999.
- [43] L. Zheng, W.-L. Chiang, Y. Sheng, S. Zhuang, Z. Wu, Y. Zhuang, Z. Lin, Z. Li, D. Li, E. Xing, et al. Judging llm-as-a-judge with mt-bench and chatbot arena. *Advances in neural information processing systems*, 36:46595–46623, 2023.
- [44] K. Zou, Z. Huang, Y. Dong, S. Tian, D. Zheng, H. Liu, J. He, B. Liu, Y. Qiao, and Z. Liu. Uni-mmmu: A massive multi-discipline multimodal unified benchmark, 2026. URL <https://arxiv.org/abs/2510.13759>.

## A. Benchmark Details

### A.1. Task Taxonomy

The Polaris-Bench comprises 53 procedurally generated visual reasoning tasks, each yielding 200 QA pairs (100 Cartesian + 100 Polar), totaling 10,800 QA pairs across the suite (Word Search additionally includes Hexagonal and Octagonal variants, contributing 400 QA pairs). We organize these tasks into five cognitive domains based on the core reasoning ability each task primarily evaluates:

- **Visual Pattern Matching** (11 tasks) evaluates pattern recognition and structural discrimination, including shape assembly, visual search, and sequential pattern continuation.
- **Spatial Transformation and Geometry** (13 tasks) evaluates geometric transformation reasoning (e.g., rotation, reflection, folding) alongside quantitative geometric measurement such as area counting and curve estimation.
- **Navigation and Routing** (14 tasks) evaluates sequential positional state tracking, requiring models to execute or trace multi-step movement paths under environmental constraints such as walls, wrapping boundaries, and monotonicity rules.
- **Combinatorics and Probability** (9 tasks) evaluates systematic combinatorial enumeration and probabilistic reasoning, including path counting under topological boundary conditions and stochastic trajectory analysis.
- **Algorithmic Logic and Simulation** (6 tasks) evaluates constraint satisfaction, discrete optimization, and deterministic forward simulation of physical or rule-based dynamics.

Tables 3–7 provide a complete per-task breakdown. For each task, we report its sub-category, answer type, a one-sentence description, and two topological properties. *Alignment* indicates whether the Cartesian and Polar versions share identical ground-truth answers (✓ = Fully Aligned) or intentionally diverge due to intrinsic topological differences (✗ = Partially Aligned). *Boundary* specifies the Polar layout’s boundary condition: *Bounded* (closed, non-wrapping edges), *Wrapping* (360° angular wrap-around), or “—” (topology-invariant tasks unaffected by the boundary condition). Figure 8 provides a statistic of task distribution among answer type, alignment between Cartesian and Polar, and boundary condition.

**Partially Aligned Tasks** Below we provide task-specific explanation to partial aligned tasks, where the Cartesian and Polar instances share same problem rules, but the valid solution and ground-truth answers are different:

- **Impossible Shape.** Finding a perfectly identical shape correspondence between Cartesian (rectangular cells) and Polar (sector-shaped cells) layouts is inherently infeasible. We therefore control for identical grid dimensions and overall shape silhouette, but due to the geometric differences between cell types, the set of valid rotation and assembly configurations may differ.
- **Knight Paths.** Under identical problem setups, the Polar layout permits angular wrapping, granting the knight additional boundary-crossing moves that do not exist on a bounded Cartesian grid. This results in more valid paths to reach the destination in Polar.
- **Longest Path.** The set of candidate paths and the correct answer are identical across both versions. However, to prevent candidate paths from inadvertently connecting head-to-tail through angular wrapping, the Polar layout uses one additional sector compared to the number of Cartesian columns.

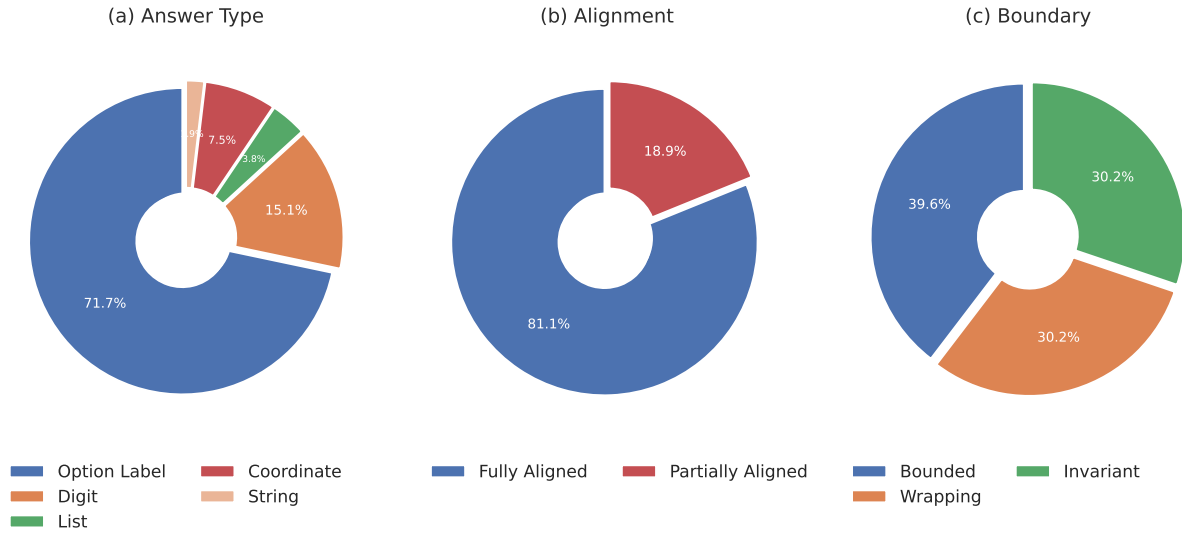


Figure 8 | Task distribution of Polaris-Bench across (a) answer type, (b) alignment, (c) boundary condition.

- **Maximum Collection.** The Polar layout permits angular wrapping, expanding the reachable region along the trajectory. Consequently, more numbers can be collected in Polar under the same movement rules, yielding a higher optimal collection value.
- **Minimum Flips.** Angular wrapping makes the first and last columns effectively adjacent, introducing additional parity constraints on the boundary. This alters the minimum number of flips required to achieve the target pattern.
- **Random Walk.** The problem formulation and correct answer are kept identical across both versions. To achieve answer alignment despite wrapping, the Polar layout uses a slightly larger number of sectors, with the key intersections (A, B, C) placed within a contiguous sector region whose internal connectivity mirrors that of the Cartesian grid.
- **Rotation Center.** To ensure that the answer and key point positions align correctly between the two coordinate systems, the Polar grid uses a different grid size from the Cartesian version.
- **Wrapping Diagonal Path.** Angular wrapping in Polar allows diagonal paths to wrap around the angular boundary, creating additional valid trajectories that do not exist in the bounded Cartesian grid. This increases the total count of valid diagonal paths.

## B. Benchmark Construction Details

### B.1. Visual Calibration

The Polar coordinate mapping introduces nonlinear spatial distortion that can systematically disadvantage model perception if left unaddressed. We apply task-specific visual calibrations to ensure that critical visual elements remain perceptually comparable across Cartesian and Polar layouts.

For example, for tasks where font size is a key perceptual factor (e.g., word search, odd one out), we enforce matched letter sizes across both layouts. Since Polar cells near the pole are significantly compressed, we adjust the Polar rendering to use cells large enough for legible text. To maintain size parity, we correspondingly introduce additional white space in the Cartesian layout, forcing the core visual elements (i.e., the letters) to occupy a comparable rendered area rather than filling the entire grid. This ensures that any performance gap reflects reasoning difficulty rather than a legibility

Table 3 | Details of 11 tasks for the **Visual Pattern Matching** domain. Each task yields 200 QA pairs (100 Cartesian + 100 Polar) unless otherwise noted.

| Task Name          | Sub-Category               | Answer Type  | Description  | #QA | Alignment | Boundary |
|--------------------|----------------------------|--------------|--|-----|-----------|----------|
| Pattern Completion | Shape and Jigsaw Assembly  | Option label | Fill a missing contiguous region in a bi-color diagonally partitioned layout   | 200 | ✓         | —        |
| Shape Fitting      | Shape and Jigsaw Assembly  | Option label | Choose the piece that exactly fills an irregular hole in a cell layout         | 200 | ✓         | Bounded  |
| Layer Completion   | Shape and Jigsaw Assembly  | Option label | Select the piece that fills a missing chunk in a concentric-layer colored grid | 200 | ✓         | Bounded  |
| Fragment Matching  | Shape and Jigsaw Assembly  | Option label | Match a grid fragment to a hole based on non-uniform line spacing patterns     | 200 | ✓         | —        |
| Template Matching  | Shape and Jigsaw Assembly  | Option label | Find which puzzle piece (with rotation/flip) is hidden in a symbol grid        | 200 | ✓         | Wrapping |
| Jigsaw Matching    | Shape and Jigsaw Assembly  | Option label | Determine which two of four pieces combine to form a complete shape            | 200 | ✓         | Bounded  |
| Shape Completion   | Shape and Jigsaw Assembly  | Option label | Identify which piece fills the missing gap to complete a solid shape           | 200 | ✓         | Wrapping |
| Odd Piece Out      | Visual Spotting and Search | Option label | Find the imposter piece that doesn't fit when assembling 4 pieces into a shape | 200 | ✓         | —        |
| Anomaly Detection  | Visual Spotting and Search | Coordinate   | Find the one subtly different item in a large grid of identical items          | 200 | ✓         | —        |
| Letter Collection  | Visual Spotting and Search | String       | Walk along a spiral path and collect letters only on your right-hand side      | 200 | ✓         | Wrapping |
| Pattern Prediction | Pattern Continuation       | Option label | Predict which point lies on a continuing periodic bump pattern                 | 200 | ✓         | Wrapping |

disadvantage.

For tasks involving geometric shapes or icons, we apply analogous area-matching calibrations: element sizes in Cartesian layouts are scaled to approximate the rendered area of their Polar counterparts, rather than naively filling the available cell space. These calibrations are tuned on a per-task basis through manual inspection.

## B.2. Procedural Generation

Each of the 53 tasks is implemented as a self-contained Python script that procedurally generates paired Cartesian–Polar instances. The generation process involves several carefully tuned components.

**Randomization Tuning.** We randomize multiple axes per task, including grid dimensions, starting positions, path topologies, target placements, distractor counts, and color palettes. The randomization bounds for each axis were manually calibrated through iterative testing to satisfy two constraints simultaneously: (1) all generated instances must be solvable with a unique correct answer, and (2) no configuration should produce visual elements that are too small or cluttered to be perceived, particularly under Polar distortion. This tuning process was performed by the authors through systematic manual review.

**Solvability and Corner Case Resolution.** Each script includes programmatic solvability checks that verify the generated instance has a valid, unique solution before it is accepted. Beyond these automated checks, we conducted extensive manual and LLM-assisted reviews to identify and resolve

Table 4 | Task details for the **Spatial Transformation and Geometry** domain (13 tasks). Notation follows Table 3.

| Task Name         | Sub-Category                       | Answer Type  | Description   | #QA   | Alignment | Boundary |          |
|-------------------|------------------------------------|--------------|---|---|-----------|----------|----------|
| Rotation Matching | Rotations and Reflections          | List         | Match 3 rotated versions of a colored ring/polygon pattern to 6 candidates      | 200   | ✓         | Wrapping |          |
| Mirror Reflection | Rotations and Reflections          | Option label | Identify the correct mirror reflection of a half-filled colored layout          | 200   | ✓         | Bounded  |          |
| Grid Rotation     | Rotations and Reflections          | Option label | Identify a grid’s appearance after a 90° rotation from 5 options                | 200   | ✓         | —        |          |
| Rotation Center   | Rotations and Reflections          | Option label | Determine which point is the center of rotation between two segments            | 200   | ✗         | —        |          |
| Pivot Rotation    | Rotations and Reflections          | Option label | Identify the appearance of a shape after 180° rotation around a marked pivot    | 200   | ✓         | —        |          |
| Impossible Shape  | Spatial straint Topology           | Con-and      | Option label  | Find which combined grid cannot be made by inserting a piece into a frame     | 200       | ✗        | Wrapping |
| Grid Folding      | Spatial straint Topology           | Con-and      | Option label  | Fold a grid along a line; find which labeled cell is not covered              | 200       | ✓        | Bounded  |
| Four-Color        | Spatial straint Topology           | Con-and      | Option label  | Insert a colored connected piece into a gap without violating adjacency rules | 200       | ✓        | —        |
| Area Counting     | Geometric Measurement and Counting | Digit        | Count the number of gray shaded cells forming a connected region                | 200   | ✓         | Bounded  |          |
| Pipe Lengths      | Geometric Measurement and Counting | List         | Count the lengths of colored pipes filling a layout; report in descending order | 200   | ✓         | —        |          |
| Uncut Cells       | Geometric Measurement and Counting | Option label | Count cells not intersected by two boundary-spanning diagonal cuts              | 200   | ✓         | Bounded  |          |
| Area Balancing    | Geometric Measurement and Counting | Option label | Choose the cell pattern that makes total black area equal total white area      | 200   | ✓         | —        |          |
| Curve Length      | Geometric Measurement and Counting | Option label | Calculate the total length of a snake tracing cell boundary edges               | 200   | ✓         | —        |          |

corner cases. For example, we discovered through literature review that N-Queens under wrapping (i.e., toroidal) boundary conditions has no valid solution for most board sizes; we therefore constrained this task to use bounded topology exclusively. Similar task-specific adaptations were applied across the benchmark wherever edge cases were identified.

**Distractor Validation.** For tasks with multiple-choice or enumeration-based answers, we implement explicit distractor validation to ensure that incorrect answer options are genuinely incorrect. The generative scripts verify that each distractor does not accidentally coincide with the ground-truth answer under alternative interpretations or boundary conditions. This prevents ambiguous evaluation where a model might select a “wrong” answer that is in fact defensible.

Table 5 | Task details for the **Navigation and Routing** domain (14 tasks). Notation follows Table 3.

| Task Name             | Sub-Category             | Answer Type  | Description  | #QA | Alignment | Boundary |
|-----------------------|--------------------------|--------------|--|-----|-----------|----------|
| Maze                  | Optimal Pathfinding      | Option label | Find which labeled entrance leads to the exit through a maze                               | 200 | ✓         | Bounded  |
| Shortest Path         | Optimal Pathfinding      | Option label | Compare 4 diagonal zigzag routes and find the shortest (or all-equal)                      | 200 | ✓         | —        |
| Longest Path          | Optimal Pathfinding      | Option label | Compare 5 paths on grids and identify which is the longest                                 | 200 | ✗         | Bounded  |
| Bounded Path Finding  | Optimal Pathfinding      | Option label | Select the correct move sequence for a penguin reaching a fish on a bounded grid           | 200 | ✓         | Bounded  |
| Wrapping Path Finding | Optimal Pathfinding      | Option label | Select the correct move sequence on a cylindrical wrapping grid                            | 200 | ✓         | Wrapping |
| Wrapping Navigation   | Rule-Based Navigation    | Option label | Trace an absolute-direction movement sequence on a wrapping grid to find the target animal | 200 | ✓         | Wrapping |
| Egocentric Navigation | Rule-Based Navigation    | Option label | Mouse traces egocentric commands (Fwd/Back/Turn) through cacti to find food                | 200 | ✓         | Bounded  |
| Absolute Navigation   | Rule-Based Navigation    | Option label | Turtle traces absolute directions through cacti to find flowers (bounded)                  | 200 | ✓         | Bounded  |
| Wall Follower         | Rule-Based Navigation    | Coordinate   | Simulate a robot that turns right at walls; find where it stops or loops                   | 200 | ✓         | Bounded  |
| Rule-Based Navigation | Rule-Based Navigation    | Coordinate   | Simulate a drone with alternating R/L banking rules; find where it lands                   | 200 | ✗         | Bounded  |
| Monotonic Path        | Constraint-Based Routing | Option label | Navigate rooms with strictly increasing numbers from START to the correct exit             | 200 | ✓         | Wrapping |
| Turn Counting         | Constraint-Based Routing | Option label | Identify the path with the exact specified number of left and right turns                  | 200 | ✓         | Bounded  |
| Word Search           | Constraint-Based Routing | Digit        | Count valid adjacent-cell paths that spell a target word from the center                   | 400 | ✓         | —        |
| Largest Number Path   | Constraint-Based Routing | Option label | Trace digit paths through a number grid; identify which forms the largest number           | 200 | ✓         | —        |

### B.3. Rendering and Legibility

Rendering Polar layouts introduces several unique visual challenges that require dedicated engineering solutions.

**Anti-Collision Constraints.** We enforce strict anti-collision rules to prevent overlapping visual elements. Grid lines, labels, icons, and path traces are rendered with minimum separation guarantees. Under Polar distortion, cells near the pole are significantly smaller than those near the boundary; we dynamically adjust label placement and font sizing to prevent overlap in these compressed regions.

**Boundary Wrapping Artifacts.** Certain visual patterns that appear straightforward in Cartesian layouts create rendering artifacts under Polar mapping. For instance, a polyline that spans both the left and right edges of a Cartesian grid will form a closed circle in Polar space, fundamentally altering its visual appearance. We address such cases through multiple strategies: constraining the generative script to produce polylines that touch at most one boundary, adding an extra column to the Polar layout to break the visual closure, or programmatically detecting and excluding instances where unwanted closed loops arise.

Table 6 | Task details for the **Combinatorics and Probability** domain (9 tasks). Notation follows Table 3.

| Task Name               | Sub-Category              | Answer Type  | Description   | #QA | Alignment | Boundary |
|-------------------------|---------------------------|--------------|---|-----|-----------|----------|
| Path Counting           | Bounded Combinatorics     | Option label | Count distinct shortest paths from P to Q avoiding wall obstacles                       | 200 | ✓         | Bounded  |
| Bounded Diagonal Paths  | Bounded Combinatorics     | Digit        | Count diagonal paths from P to Q with a wall blocking Polar wrap-around                 | 200 | ✓         | Bounded  |
| Bounded Knight Paths    | Bounded Combinatorics     | Digit        | Count knight paths from start to target with a wall blocking sector wrap-around         | 200 | ✓         | Bounded  |
| Checkpoint Paths        | Bounded Combinatorics     | Digit        | Count right/down paths from X to Y passing through checkpoint $\nabla$ , avoiding gaps  | 200 | ✓         | Bounded  |
| Lattice Paths           | Bounded Combinatorics     | Digit        | Count paths on a dot grid allowing right, down, and diagonal-down-right moves           | 200 | ✓         | Bounded  |
| Wrapping Diagonal Paths | Topological Combinatorics | Digit        | Count diagonal paths from P to Q on an alternating-color layout with wrapping           | 200 | ✗         | Wrapping |
| Knight Paths            | Topological Combinatorics | Digit        | Count paths for a chess knight from start to target in exactly K steps                  | 200 | ✗         | Wrapping |
| Edge Counting           | Stochastic Processes      | Option label | Count the number of cell edges an ant traverses from P to Q                             | 200 | ✓         | —        |
| Random Walk             | Stochastic Processes      | Option label | Calculate the probability of passing through point C on a random walk $A \rightarrow B$ | 200 | ✗         | Wrapping |

**Inner Ring Radius Optimization.** If the inner ring radius is too small, elements near the pole become illegibly compressed; if too large, the outer rings waste space. We tune the inner ring radius on a per-task basis to find the optimal balance between visual clarity near the pole and efficient use of the rendering canvas. This parameter is adjusted through manual inspection of representative instances for each task.

#### B.4. Quality Assurance Pipeline

Our quality assurance process consists of three iterative stages followed by a final human validation study.

**Author Review.** The authors collaboratively reviewed the logical design of each task, verifying that the rules, constraints, and ground-truth computations are correct for both Cartesian and Polar versions. In addition, we independently spot-checked randomly sampled instances for each of the 53 tasks by manually solving them and comparing our answers against the computed ground truths.

**LLM-Assisted Code Audit.** We used Gemini-3.1-Pro to systematically audit the procedural generation code, prompting the model to identify potential edge cases, off-by-one errors, and boundary condition failures. This process surfaced several subtle bugs that were not apparent during manual review, including incorrect wrapping behavior at grid boundaries and degenerate configurations for specific grid dimensions.

**Iterative Convergence.** The above two stages were repeated in multiple rounds. Each round produced a list of identified issues, which were resolved before the next round of review. This process continued until no further issues were identified across all 53 tasks.

Table 7 | Task details for the **Algorithmic Logic and Simulation** domain (6 tasks). Notation follows Table 3.

| Task Name           | Sub-Category                     | Answer Type  | Description  | #QA | Alignment | Boundary |
|---------------------|----------------------------------|--------------|--|-----|-----------|----------|
| N-Queens            | Constraint Satisfaction          | Option label | Place missing queens on a partial N-Queens board; deduce the target coordinate           | 200 | ✓         | Bounded  |
| Sudoku              | Constraint Satisfaction          | Option label | Solve for the value of a highlighted cell in a partially filled Sudoku                   | 200 | ✓         | —        |
| Minimum Flips       | Move Optimization                | Option label | Find minimum moves to achieve an alternating two-color pattern by flipping 3-cell strips | 200 | ✗         | Wrapping |
| Maximum Collection  | Move Optimization                | Option label | Find the maximum cheese a mouse can eat on a non-repeating maze path                     | 200 | ✗         | Wrapping |
| Collision Detection | Motion and Trajectory Prediction | Option label | Determine which pair of moving cars will crash first based on velocity arrows            | 200 | ✓         | Wrapping |
| Bouncing Point      | Motion and Trajectory Prediction | Coordinate   | Compute coordinates after N steps of a bouncing/looping point                            | 200 | ✗         | Wrapping |

**Representative Examples of Resolved Issues.** To illustrate the depth of this process, we highlight several representative cases:

- *N-Queens wrapping*: Literature review revealed that N-Queens under toroidal (wrapping) boundary conditions has no valid solution for most board sizes. We adapted this task to use bounded topology exclusively.
- *Polyline boundary closure*: Polylines spanning both edges of a Cartesian grid form closed circles under Polar mapping. We constrained generation to avoid this artifact (Section B.3).
- *Distractor collision*: In several combinatorial tasks, randomly generated distractors occasionally coincided with the correct answer under alternative boundary interpretations. We added explicit distractor validation checks to eliminate these cases.

**Representative Design Refinements.** Beyond resolving correctness issues, we iteratively refined task designs in this tag based on observations and results, for more comprehensive evaluation and reduce possible shortcut for answering. Below are some representative examples:

- *Four Color*: This task originally used numerical labels (1–4) to fill cells, presenting a layout close to the Monotonic Path task. Pilot evaluation revealed that both tasks exhibited similarly high accuracy across Cartesian and Polar layouts. After comparative analysis on their CoT reasoning chain, we retained numerical labels for monotonic path and switched four color to use color-filled cells, creating a controlled contrast pair. Under this design, four color exhibits sharp performance collapse on Polar layouts, further corroborating our analysis of why Monotonic Path resists the topology shift (Section 5).
- *Letter Collection*: This task was originally framed as multiple-choice. We observed that models could exploit an elimination strategy: identifying letters unique to each option, finding them on the image and verifying their positioning correctness, rather than genuinely tracing the path to collect letters. We reformulated the task to require sequential string output, forcing models to actually traverse the path and aggregate the collected letters in order. This adjustment caused a sharp performance decline, confirming that the original format permitted a reasoning shortcut. Notably, under the multiple-choice setting, increasing the length of candidate strings does not

degrade performance, indicating that the difficulty of the underlying task is not really be evaluated in the multi-choice setting. After converting to string output format, we subsequently reduced task difficulty in multiple iterations to ensure performance remained sufficiently above the random baseline to yield informative signal.

## B.5. Human Validation Study

As a final safeguard, we conducted a human validation study to confirm the quality of the benchmark data. For each of the 53 tasks, we randomly sampled 20 Cartesian–Polar paired instances and presented them to independent human raters. For each instance, raters were asked to evaluate the following three criteria:

1. **Visual clarity:** Is the rendered image visually clear and legible? Can all relevant elements (labels, shapes, paths, grid lines) be unambiguously perceived?
2. **Logical correctness:** Is the task logic (rules, constraints, problem formulation) consistent and well-defined?
3. **Answer correctness:** Is the provided ground-truth answer correct? (Options: *Correct*, *Incorrect*, *I don't know*.)

## C. Evaluation Setup Details

### C.1. Model Query Details

All models are evaluated via their publicly available APIs using default generation configurations to ensure optimal performance. We set the maximum output token limit to each model’s maximum supported value. For the Gemini, GPT, Grok and Gemma model families, we query their respective first-party APIs. For all remaining models (e.g., Qwen, Kimi, Mistral), we access them through third-party serving platforms, specifically TogetherAI and OpenRouter.

**Reasoning Mode Configuration.** For models supporting configurable reasoning, we evaluate under two inference settings: (1) a *high reasoning* mode that activates the model’s highest supported reasoning budget, and (2) a *non-reasoning* mode that uses the minimal reasoning configuration. We note the following model-specific exceptions:

- **Gemini-3.1-Pro** [16]: Gemini-3.1-Pro does not support a fully non-reasoning setting. We therefore report its non-reasoning results under the low reasoning budget (reasoning set to LOW).
- **Claude-Sonnet-4.6** [2]: Due to query timeouts under the extended high reasoning mode, the high reasoning results reported in this paper are obtained using the default adaptive high reasoning mode.
- **Grok-4-Fast-Reasoning** [35]: We pair Grok-4-Fast-Reasoning and Grok-4-Fast-Non-Reasoning as the high reasoning and non-reasoning variants, respectively, in Table 2.

### C.2. Evaluation Setup for the Cartesian Shortcut

Here we provide implementation details for the empirical analyses presented in Section 2.

**Chain-of-Thought Discretization Analysis.** To quantify how frequently models discretize visual layouts into textual coordinates during reasoning, we conduct a Chain-of-Thought (CoT) analysis across 9 prominent visual reasoning benchmarks: BabyVision [8], OmniSpatial [19], EMMA [18], MegaBench [6], MMMU-Pro [41], BLINK [12], CharXiv [33], MUIRBench [32], and MMIU [22]. We use Gemini-3-Flash as a representative model. To isolate synthetic, grid-based visual reasoning tasks, we first prompt the model to filter out photographic images and examples with domain-specific backgrounds (e.g., medical imaging, charts), yielding over 3,800 qualifying examples. We then evaluate these examples under the high reasoning mode of Gemini-3-Flash and collect the intermediate Chain-of-Thought outputs. To systematically detect spatial discretization, we provide the generated reasoning traces to Gemini-3.1-Pro as a judge, prompting it to identify whether the reasoning explicitly invokes Cartesian coordinates or axis-aligned positional references (e.g., “row 2”, “column 3”, “(x,y)”). Results show that 56.58% of examples exhibit explicit Cartesian coordinate usage in their reasoning traces, confirming the prevalence of the Cartesian Shortcut.

**Two-Stage Perception-Reasoning Disentanglement.** To further isolate the role of visual perception from deductive reasoning, we conduct a two-stage experiment on Gemini-3.1-Pro (Figure 1). In the first stage, we provide only the task image and prompt the model to generate a detailed descriptive caption, explicitly informing the model that this caption will subsequently be used to answer a question. In the second stage, we provide the original question together with the generated caption (without the image) and prompt the model to answer based solely on the textual description. To evaluate caption quality, we use the grid dimensions as a proxy for perceptual accuracy: we extract the ground-truth grid size from each example’s metadata and prompt Gemini-3.1-Pro to verify whether the caption correctly reports the grid dimensions. We clarify that comprehensively evaluating caption fidelity would require manual human inspection; grid size verification serves as a coarse but scalable proxy for perceptual accuracy rather than a precise measure. A caption is marked as incorrect if it explicitly mentions a grid size that contradicts the ground truth. As reported in Figure 1, grid size extraction accuracy reaches 80.2% on Cartesian layouts but drops to only 20.8% on Polar layouts. Crucially, when evaluating task accuracy exclusively on the subset of correctly perceived instances, Cartesian examples maintain 86.9% accuracy while Polar examples collapse to 47.6%, demonstrating that the performance gap persists even when visual perception is controlled for.

### C.3. Evaluation Prompt Template

```

Please answer the following question based on the image.
Output **only the final correct answer directly**, nothing else is allowed in the
output. e.g., for multi-choise, it can only contain option letter (e.g., A). For
text answers, it can only contain the required answer values.

[Question]
{Question}
<img>

```

Figure 9 | Prompt template used in the standard evaluation in our experiments.

All tasks across both Cartesian and Polar layouts share a unified evaluation prompt template to ensure fair comparison. The template consists of: (1) a task-specific narrative providing contextual framing and rules, (2) the visual input image, and (3) the question with its answer format specification.

```

Please answer the following question based on the image.
Put your analysis before the correct answer. In the last line, make sure provide
only the correct answer, nothing else is allowed in last line. **Last line must
only contain correct answer as question asked.**

[Task Hint]
The image displays a polar (radial) layout. This is topologically equivalent to a
standard rectangular grid: each concentric ring corresponds to a row, and each
angular sector corresponds to a column. To solve this problem, first reconstruct
the equivalent Cartesian grid by reading the content of each cell (ring, sector)
and mapping it into the corresponding (row, column) position in a matrix. Then,
solve the problem on this reconstructed matrix using standard
grid-based reasoning.

[Question]
{Question}
<img>

```

Figure 10 | Prompt template used in conversion hint experiment.

The exact prompt template is provided in Figure 9.

For the out-of-distribution interventions described in Section 5, we employ two additional prompt variants:

- **Conversion Hint:** The prompt is augmented with an explicit instruction asking the model to first re-map the Polar layout into an equivalent Cartesian grid representation before attempting to solve the task.
- **5-Shot In-Context Learning:** The prompt is prepended with five solved Polar examples from the same task, each consisting of the Polar image, the question, and the correct answer, to scaffold the model’s reasoning on Polar layouts.

The exact prompts for these two variants are provided in Figure 10 and Figure 11 respectively..

#### C.4. Evaluation Metrics

All tasks in the Polaris-Bench are designed with deterministic, well-defined answer formats, enabling reliable automated evaluation. Depending on the task, ground-truth answers take one of the following standardized forms: multiple-choice labels, exact integers, coordinate pairs or axis positions, ordered lists, and directional sequences, as stated in Section A.1. In this case, we employ rule-based programmatic parsers as the primary evaluation method. For each answer format, a dedicated parser extracts the model’s predicted answer from its response and performs an exact-match comparison against the ground truth. Across all evaluated models, the vast majority of responses are successfully parsed and evaluated through this automated pipeline. For the small fraction of responses where programmatic parsing fails, typically due to models not following the specified output format instructions, we apply an LLM-as-a-judge [17, 43] as a calibration fallback. Specifically, we prompt Gemini-3.1-Pro with both the ground-truth answer and the model’s raw response, and ask it to determine whether the response is correct. This two-tier evaluation strategy ensures that models are not unfairly penalized for minor formatting deviations while maintaining rigorous evaluation standards.

```

You are a visual reasoning expert. Below are examples of how to analyze and solve
specific spatial tasks.

[Examples]
{few_shot_text}

[Task Instruction]
Please solve the following new question based on the provided question image.
1. Think step-by-step about the spatial layout and rules. Use above examples as
reference.
2. Output your final answer clearly on the very last line.

Ensure your response strictly follows this structure:
<Analysis>
(Your step-by-step reasoning here)
</Analysis>
(Your final exact answer here, on the absolute last line)

[Question]
{Question}
<img>

```

Figure 11 | Prompt template used in the few-shot in context learning.

**Random Baseline.** We additionally report a theoretical random baseline computed from the statistical expectation of each task’s answer format. For multiple-choice tasks, this corresponds to  $1/k$  where  $k$  is the number of options; for integer and coordinate tasks, the baseline is derived from the uniform distribution over the valid answer space. This baseline serves as a lower-bound reference to contextualize model performance.

### C.5. Evaluation Results Statistic

All results reported in this work are based on a single evaluation run per model. The main reason is the substantial computational cost of evaluation. The 53 tasks in Polaris-Bench require complex visual reasoning, especially the main results of models under high reasoning mode, frequently engage in long time thinkings, which results in several minutes of inference times and consuming large output token budgets. In some cases, it even reach the maximum output token limit without coming out a answer, we rerun the examples in this case. Thus, a single model’s evaluation reveal a very high cost. Due to this, we report the results on single run. Meanwhile, we leverage below for results robustness:

**Spot-check verification.** We conduct spot-check experiments on core models across randomly sampled tasks with multiple runs. The accuracy variations are within a reasonably small percentage points across runs (e.g., Gemini 3.1 Pro on four color, accuracy of two runs under exactly same setting: (0.92, 0.33) and (0.9, 0.3) for Cartesian and Polar respectively.)

Furthermore, the following factors also support the robustness of our results:

- **Large sample size.** Each task has 100 paired Cartesian–Polar instances. Aggregate results are computed over 5,300 instances per coordinate condition, which reduces instance-level noise.

- **Large effect sizes.** The Cartesian-to-Polar drops are 30–50 percentage points (Table 1). A run-to-run variance of  $\pm 3$  points, as observed in our spot-check, does not change any conclusion.
- **Cross-model consistency.** The same collapse pattern appears across all 14 models from 8 different families, spanning proprietary and open-source. Each model is an independent observation of the same phenomenon.
- **Consistency across conditions.** The collapse is consistent across five task categories (Table 1), fully vs. partially aligned tasks (Figure 5(a)), bounded vs. wrapping conditions (Figure 5(b)), and reasoning vs. non-reasoning modes (Table 2).

## D. Complete Experimental Results

### D.1. Overall Performance Analysis

We provide fine-grained radar chart visualizations to complement the aggregate results reported in Table 1 and Table 2. These charts display per-category accuracy across the five task taxonomies (i.e., visual pattern matching, spatial transformation and geometry, navigation and routing, combinatorics and probability, and algorithmic logic and simulation) enabling direct visual comparison of model performance profiles.

Figure 12 presents the per-category performance of all evaluated models under high reasoning mode, separated into closed-source (top row) and open-source (bottom row) groups. The left column shows Cartesian accuracy and the right column shows Polar accuracy. On Cartesian layouts, closed-source models exhibit relatively expanded and overlapping radar profiles, with Gemini-3.1-Pro achieving the largest coverage. On Polar layouts, all radar profiles contract substantially and cluster closer to the center. Among open-source models, a similar contraction pattern is observed, with Polar profiles notably smaller and more compressed than their Cartesian counterparts across all five categories.

Figures 13 and 14 present the effect of reasoning mode on per-category performance for closed-source and open-source models, respectively. Each figure contains four panels: the top row shows non-reasoning mode results on Cartesian (left) and Polar (right) layouts, while the bottom row shows the corresponding high reasoning mode results. For closed-source models (Figure 13), the radar profiles expand visibly from non-reasoning to reasoning on Cartesian layouts, whereas the expansion on Polar layouts is comparatively modest. For open-source models (Figure 14), the reasoning mode similarly produces larger radar profiles on Cartesian layouts, while the Polar profiles remain relatively compact across both reasoning settings.

Figure 15 further disaggregates model performance by answer type rather than task category, with axes corresponding to Coordinate, Digit, String, Option Label, and List. On Cartesian layouts, both closed-source and open-source models exhibit relatively expanded radar profiles with visible inter-model variation across answer types. Upon transition to Polar layouts, all profiles contract substantially, and the degree of contraction varies across answer types, indicating that the Cartesian-to-Polar performance gap is not uniform across output formats. Among open-source models, the Polar profiles are particularly compressed, with reduced inter-model differentiation compared to their Cartesian counterparts.

### D.2. Per-Catagory Breakdown Performance

We report detailed per-task performance for all five task categories, with results organized by subcategory where applicable.

Table 8 | Per-task results under the Navigation and Routing category, subcategory Rule-Based Navigation. All models are evaluated under high reasoning mode. C and P denote Cartesian and Polar accuracy (%), respectively.  $(-\Delta)$  indicates the accuracy change from Cartesian to Polar. Task abbreviations: Abs. Nav. = Absolute Navigation; Ego. Nav. = Egocentric Navigation; Rule Nav. = Rule-Based Navigation; Wall Fol. = Wall Follower; Wrap. Nav. = Wrapping Navigation.

| Model                      | Abs. Nav. |      |             | Ego. Nav. |      |             | Rule Nav. |      |             | Wall Fol. |      |             | Wrap. Nav. |      |             |
|----------------------------|-----------|------|-------------|-----------|------|-------------|-----------|------|-------------|-----------|------|-------------|------------|------|-------------|
|                            | C         | P    | $(-\Delta)$ | C         | P    | $(-\Delta)$ | C         | P    | $(-\Delta)$ | C         | P    | $(-\Delta)$ | C          | P    | $(-\Delta)$ |
| Random                     | 16.7      | 16.7 | (0.0)       | 16.7      | 16.7 | (0.0)       | 20.0      | 20.0 | (0.0)       | 20.0      | 20.0 | (0.0)       | 16.7       | 16.7 | (0.0)       |
| <i>Closed-Source MLLMs</i> |           |      |             |           |      |             |           |      |             |           |      |             |            |      |             |
| Gemini-3.1-Pro             | 96.0      | 31.0 | (-65.0)     | 94.0      | 32.0 | (-62.0)     | 95.0      | 12.0 | (-83.0)     | 89.0      | 52.5 | (-36.5)     | 99.0       | 24.5 | (-74.5)     |
| Gemini-3-Flash             | 81.0      | 16.0 | (-65.0)     | 76.0      | 21.0 | (-55.0)     | 88.0      | 29.0 | (-59.0)     | 63.0      | 19.0 | (-44.0)     | 76.0       | 25.0 | (-51.0)     |
| Gemini-3-Flash-lite        | 47.0      | 15.0 | (-32.0)     | 34.0      | 10.0 | (-24.0)     | 80.0      | 17.0 | (-63.0)     | 48.0      | 31.0 | (-17.0)     | 40.0       | 19.0 | (-21.0)     |
| Gemini-2.5-Pro             | 23.0      | 16.0 | (-7.0)      | 13.0      | 7.0  | (-6.0)      | 85.0      | 15.0 | (-70.0)     | 48.0      | 47.0 | (-1.0)      | 36.0       | 25.0 | (-11.0)     |
| Gemini-2.5-Flash           | 20.0      | 13.0 | (-7.0)      | 8.0       | 12.0 | (4.0)       | 64.0      | 16.0 | (-48.0)     | 52.0      | 50.0 | (-2.0)      | 15.0       | 15.0 | (0.0)       |
| GPT-5.2                    | 91.0      | 29.0 | (-62.0)     | 71.0      | 27.0 | (-44.0)     | 96.0      | 32.0 | (-64.0)     | 88.0      | 29.0 | (-59.0)     | 93.0       | 36.0 | (-57.0)     |
| Claude-Sonnet-4.6          | 75.3      | 23.2 | (-52.1)     | 43.8      | 17.4 | (-26.5)     | 24.7      | 19.8 | (-5.0)      | 42.7      | 23.7 | (-19.0)     | 52.0       | 21.2 | (-30.8)     |
| Grok-4-0709                | 19.0      | 13.0 | (-6.0)      | 9.0       | 6.0  | (-3.0)      | 61.6      | 10.0 | (-51.6)     | 47.0      | 42.0 | (-5.0)      | 16.0       | 16.0 | (0.0)       |
| Grok-4-Fast-Reasoning      | 25.0      | 25.0 | (0.0)       | 21.0      | 28.0 | (7.0)       | 56.0      | 31.0 | (-25.0)     | 23.0      | 23.0 | (0.0)       | 21.0       | 28.0 | (7.0)       |
| <i>Open-Source MLLMs</i>   |           |      |             |           |      |             |           |      |             |           |      |             |            |      |             |
| Gemma-4-31B                | 75.0      | 15.0 | (-60.0)     | 52.0      | 22.0 | (-30.0)     | 75.0      | 12.0 | (-63.0)     | 55.0      | 48.0 | (-7.0)      | 71.0       | 28.0 | (-43.0)     |
| Gemma-4-26B                | 52.0      | 8.0  | (-44.0)     | 13.1      | 9.0  | (-4.1)      | 66.0      | 11.0 | (-55.0)     | 44.0      | 37.0 | (-7.0)      | 59.0       | 10.0 | (-49.0)     |
| Kimi-k2.5                  | 94.9      | 27.4 | (-67.5)     | 93.0      | 16.3 | (-76.7)     | 83.0      | 26.0 | (-57.0)     | 53.0      | 28.0 | (-25.0)     | 95.0       | 26.0 | (-69.0)     |
| Qwen3.5-397B-A17B          | 95.0      | 17.0 | (-78.0)     | 95.0      | 25.0 | (-70.0)     | 80.0      | 14.0 | (-66.0)     | 73.0      | 40.0 | (-33.0)     | 91.0       | 33.0 | (-58.0)     |
| Mistral-Small-2503         | 23.9      | 21.3 | (-2.6)      | 6.1       | 8.1  | (2.0)       | 7.0       | 17.0 | (10.0)      | 51.0      | 51.0 | (0.0)       | 20.0       | 34.0 | (14.0)      |

**Navigation and Routing.** Tables 8, 9, and 10 present the per-task results under this category, grouped by the Rule-Based Navigation, Optimal Pathfinding, and Constraint-Based Routing subcategories, respectively.

**Visual Pattern Matching.** Tables 11 and 12 present the per-task results, with the latter merging subcategories that contain fewer tasks into a single table.

**Spatial Transformation and Geometry.** Tables 13, 14, and 15 present the per-task results, grouped by the Geometric Measurement and Counting, Spatial Constraints and Topology, and Rotations and Reflections subcategories, respectively.

**Algorithmic Logic and Simulation.** Table 16 presents the per-task results for this category. Due to the small number of tasks per subcategory, all results are consolidated into a single table.

**Combinatorics and Probability.** Tables 17 and 18 present the per-task results, with Table 17 covering the Bounded Combinatorics subcategory and Table 18 merging the Stochastic Processes and Topological Combinatorics subcategories.

Notably, while the overall Cartesian-to-Polar accuracy gap remains substantial across all models, each model exhibits a small subset of tasks on which its performance drop is comparatively moderate relative to other models evaluated on the same task. These task-level exceptions are largely *model-specific*: the particular tasks on which a given model shows a smaller gap differ considerably from one model to another, with little consistent overlap across the evaluated model set. We think this may

Table 9 | Per-task results under the Navigation and Routing category, subcategory Optimal Pathfinding. All models are evaluated under high reasoning mode. C and P denote Cartesian and Polar accuracy (%), respectively. ( $-\Delta$ ) indicates the accuracy change from Cartesian to Polar. Task abbreviations: Bound. Path = Bounded Path Finding; Long. Path = Longest Path; Short. Path = Shortest Path; Wrap. Path = Wrapping Path Finding.

| Model                      | Bound. Path |      |               | Long. Path |      |               | Maze |      |               | Short. Path |      |               | Wrap. Path |      |               |
|----------------------------|-------------|------|---------------|------------|------|---------------|------|------|---------------|-------------|------|---------------|------------|------|---------------|
|                            | C           | P    | ( $-\Delta$ ) | C          | P    | ( $-\Delta$ ) | C    | P    | ( $-\Delta$ ) | C           | P    | ( $-\Delta$ ) | C          | P    | ( $-\Delta$ ) |
| Random                     | 20.0        | 20.0 | (0.0)         | 20.0       | 20.0 | (0.0)         | 31.3 | 31.3 | (0.0)         | 20.0        | 20.0 | (0.0)         | 20.0       | 20.0 | (0.0)         |
| <i>Closed-Source MLLMs</i> |             |      |               |            |      |               |      |      |               |             |      |               |            |      |               |
| Gemini-3.1-Pro             | 98.0        | 37.0 | (-61.0)       | 78.0       | 55.0 | (-23.0)       | 34.0 | 37.5 | (3.5)         | 69.7        | 55.6 | (-14.1)       | 98.0       | 48.0 | (-50.0)       |
| Gemini-3-Flash             | 86.0        | 63.0 | (-23.0)       | 77.0       | 56.0 | (-21.0)       | 37.5 | 40.5 | (3.0)         | 93.0        | 73.0 | (-20.0)       | 92.0       | 74.0 | (-18.0)       |
| Gemini-3-Flash-lite        | 64.0        | 29.0 | (-35.0)       | 56.0       | 48.0 | (-8.0)        | 37.0 | 35.5 | (-1.5)        | 68.0        | 70.0 | (2.0)         | 51.0       | 27.0 | (-24.0)       |
| Gemini-2.5-Pro             | 33.0        | 23.0 | (-10.0)       | 69.0       | 46.0 | (-23.0)       | 32.0 | 37.5 | (5.5)         | 65.0        | 54.0 | (-11.0)       | 29.0       | 18.0 | (-11.0)       |
| Gemini-2.5-Flash           | 29.0        | 21.0 | (-8.0)        | 48.0       | 32.0 | (-16.0)       | 39.5 | 39.0 | (-0.5)        | 46.0        | 43.0 | (-3.0)        | 31.0       | 20.0 | (-11.0)       |
| GPT-5.2                    | 86.0        | 31.0 | (-55.0)       | 80.0       | 69.0 | (-11.0)       | 44.5 | 36.5 | (-8.0)        | 82.0        | 87.0 | (5.0)         | 97.0       | 32.0 | (-65.0)       |
| Claude-Sonnet-4.6          | 59.8        | 49.0 | (-10.8)       | 48.5       | 44.4 | (-4.0)        | 34.7 | 33.7 | (-1.0)        | 65.0        | 56.1 | (-8.9)        | 56.0       | 54.1 | (-1.9)        |
| Grok-4-0709                | 20.0        | 25.0 | (5.0)         | 43.4       | 40.8 | (-2.6)        | 39.5 | 32.0 | (-7.5)        | 40.0        | 43.0 | (3.0)         | 29.0       | 33.0 | (4.0)         |
| Grok-4-Fast-Reasoning      | 29.0        | 25.0 | (-4.0)        | 37.0       | 40.0 | (3.0)         | 33.5 | 39.0 | (5.5)         | 41.0        | 40.0 | (-1.0)        | 22.0       | 13.0 | (-9.0)        |
| <i>Open-Source MLLMs</i>   |             |      |               |            |      |               |      |      |               |             |      |               |            |      |               |
| Gemma-4-31B                | 72.0        | 41.0 | (-31.0)       | 71.0       | 50.0 | (-21.0)       | 42.0 | 34.0 | (-8.0)        | 62.0        | 66.0 | (4.0)         | 72.0       | 43.0 | (-29.0)       |
| Gemma-4-26B                | 48.0        | 20.2 | (-27.8)       | 48.0       | 26.0 | (-22.0)       | 27.5 | 35.0 | (7.5)         | 49.0        | 52.0 | (3.0)         | 43.4       | 30.0 | (-13.4)       |
| Kimi-k2.5                  | 93.0        | 47.0 | (-46.0)       | 68.0       | 40.8 | (-27.2)       | 43.2 | 35.7 | (-7.5)        | 68.0        | 65.0 | (-3.0)        | 90.0       | 51.0 | (-39.0)       |
| Qwen3.5-397B-A17B          | 92.0        | 52.0 | (-40.0)       | 76.0       | 57.0 | (-19.0)       | 38.5 | 42.5 | (4.0)         | 66.0        | 58.0 | (-8.0)        | 88.0       | 45.0 | (-43.0)       |
| Mistral-Small-2503         | 17.2        | 8.1  | (-9.1)        | 30.0       | 28.0 | (-2.0)        | 53.5 | 26.5 | (-27.0)       | 40.0        | 40.0 | (0.0)         | 19.0       | 16.0 | (-3.0)        |

stem from idiosyncratic biases in individual models’ training distributions. Moreover, the rare cases in which Polar accuracy approaches Cartesian accuracy almost exclusively occur when both values are near the random baseline, indicating that the model is effectively guessing under both layouts rather than demonstrating genuine resilience to topological change.

## E. Task Examples

We provide examples with complete image and question, answer from more tasks in Polaris-Bench.

Table 10 | Per-task results under the Navigation and Routing category, subcategory Constraint-Based Routing. All models are evaluated under high reasoning mode. C and P denote Cartesian and Polar accuracy (%), respectively. ( $-\Delta$ ) indicates the accuracy change from Cartesian to Polar. Task abbreviations: Lrg. Num. = Largest Number Path; Mono. Path = Monotonic Path; Turn Cnt. = Turn Counting; Word Srch. = Word Search.

| Model                      | Lrg. Num. |      |               | Mono. Path |      |               | Turn Cnt. |      |               | Word Srch. |      |               |
|----------------------------|-----------|------|---------------|------------|------|---------------|-----------|------|---------------|------------|------|---------------|
|                            | C         | P    | ( $-\Delta$ ) | C          | P    | ( $-\Delta$ ) | C         | P    | ( $-\Delta$ ) | C          | P    | ( $-\Delta$ ) |
| Random                     | 20.0      | 20.0 | (0.0)         | 16.7       | 16.7 | (0.0)         | 20.0      | 20.0 | (0.0)         | 0.0        | 0.0  | (0.0)         |
| <i>Closed-Source MLLMs</i> |           |      |               |            |      |               |           |      |               |            |      |               |
| Gemini-3.1-Pro             | 71.0      | 29.0 | (-42.0)       | 89.0       | 91.0 | (2.0)         | 57.0      | 27.0 | (-30.0)       | 100.0      | 20.0 | (-80.0)       |
| Gemini-3-Flash             | 48.0      | 26.0 | (-22.0)       | 87.0       | 94.0 | (7.0)         | 65.0      | 23.0 | (-42.0)       | 98.0       | 27.0 | (-71.0)       |
| Gemini-3-Flash-lite        | 34.0      | 22.0 | (-12.0)       | 90.0       | 52.0 | (-38.0)       | 18.0      | 13.0 | (-5.0)        | 97.0       | 14.0 | (-83.0)       |
| Gemini-2.5-Pro             | 27.0      | 23.0 | (-4.0)        | 89.0       | 80.0 | (-9.0)        | 37.0      | 21.0 | (-16.0)       | 53.0       | 23.0 | (-30.0)       |
| Gemini-2.5-Flash           | 28.0      | 23.0 | (-5.0)        | 90.0       | 63.0 | (-27.0)       | 21.0      | 21.0 | (0.0)         | 50.0       | 7.0  | (-43.0)       |
| GPT-5.2                    | 69.0      | 29.0 | (-40.0)       | 84.0       | 93.0 | (9.0)         | 71.0      | 33.0 | (-38.0)       | 98.0       | 36.0 | (-62.0)       |
| Claude-Sonnet-4.6          | 25.3      | 19.0 | (-6.3)        | 1.0        | 0.0  | (-1.0)        | 29.0      | 24.2 | (-4.8)        | 71.6       | 13.4 | (-58.2)       |
| Grok-4-0709                | 17.0      | 22.0 | (5.0)         | 82.0       | 45.9 | (-36.1)       | 16.0      | 7.0  | (-9.0)        | 92.0       | 13.0 | (-79.0)       |
| Grok-4-Fast-Reasoning      | 23.0      | 18.0 | (-5.0)        | 86.0       | 43.0 | (-43.0)       | 21.0      | 22.0 | (1.0)         | 89.0       | 4.0  | (-85.0)       |
| <i>Open-Source MLLMs</i>   |           |      |               |            |      |               |           |      |               |            |      |               |
| Gemma-4-31B                | 31.0      | 22.0 | (-9.0)        | 84.0       | 90.0 | (6.0)         | 36.0      | 17.0 | (-19.0)       | 96.0       | 39.0 | (-57.0)       |
| Gemma-4-26B                | 27.0      | 27.0 | (0.0)         | 89.0       | 77.0 | (-12.0)       | 20.2      | 14.0 | (-6.2)        | 98.0       | 14.1 | (-83.9)       |
| Kimi-k2.5                  | 35.7      | 24.0 | (-11.7)       | 83.0       | 87.0 | (4.0)         | 25.0      | 18.0 | (-7.0)        | 96.9       | 43.4 | (-53.5)       |
| Qwen3.5-397B-A17B          | 68.0      | 34.0 | (-34.0)       | 82.0       | 94.0 | (12.0)        | 54.0      | 21.0 | (-33.0)       | 88.0       | 40.0 | (-48.0)       |
| Mistral-Small-2503         | 21.0      | 19.0 | (-2.0)        | 0.0        | 0.0  | (0.0)         | 23.0      | 16.0 | (-7.0)        | 5.0        | 12.0 | (7.0)         |

Table 11 | Per-task results under the Visual Pattern Matching category, subcategory Visual Spotting and Search / Pattern Continuation. All models are evaluated under high reasoning mode. C and P denote Cartesian and Polar accuracy (%), respectively. ( $-\Delta$ ) indicates the accuracy change from Cartesian to Polar. Task abbreviations: Anom. Det. = Anomaly Detection; Letter Col. = Letter Collection; Odd Piece = Odd Piece Out; Pat. Pred. = Pattern Prediction.

| Model                      | Anom. Det. |      |               | Letter Col. |      |               | Odd Piece |      |               | Pat. Pred. |      |               |
|----------------------------|------------|------|---------------|-------------|------|---------------|-----------|------|---------------|------------|------|---------------|
|                            | C          | P    | ( $-\Delta$ ) | C           | P    | ( $-\Delta$ ) | C         | P    | ( $-\Delta$ ) | C          | P    | ( $-\Delta$ ) |
| Random                     | 0.9        | 1.0  | (0.0)         | 0.0         | 0.0  | (0.0)         | 20.0      | 20.0 | (0.0)         | 19.7       | 19.6 | (-0.0)        |
| <i>Closed-Source MLLMs</i> |            |      |               |             |      |               |           |      |               |            |      |               |
| Gemini-3.1-Pro             | 83.0       | 10.0 | (-73.0)       | 52.0        | 37.0 | (-15.0)       | 69.0      | 42.0 | (-27.0)       | 90.0       | 27.3 | (-62.7)       |
| Gemini-3-Flash             | 78.0       | 4.0  | (-74.0)       | 36.0        | 18.0 | (-18.0)       | 65.0      | 36.0 | (-29.0)       | 83.0       | 31.0 | (-52.0)       |
| Gemini-3-Flash-lite        | 57.0       | 2.0  | (-55.0)       | 12.0        | 7.0  | (-5.0)        | 37.0      | 40.0 | (3.0)         | 32.0       | 26.0 | (-6.0)        |
| Gemini-2.5-Pro             | 27.0       | 0.0  | (-27.0)       | 6.0         | 5.0  | (-1.0)        | 36.0      | 46.0 | (10.0)        | 37.0       | 17.0 | (-20.0)       |
| Gemini-2.5-Flash           | 20.0       | 1.0  | (-19.0)       | 5.0         | 2.0  | (-3.0)        | 36.0      | 41.0 | (5.0)         | 26.0       | 29.0 | (3.0)         |
| GPT-5.2                    | 73.0       | 2.0  | (-71.0)       | 24.0        | 18.0 | (-6.0)        | 88.0      | 49.0 | (-39.0)       | 54.0       | 13.0 | (-41.0)       |
| Claude-Sonnet-4.6          | 74.8       | 1.0  | (-73.7)       | 14.1        | 5.1  | (-9.1)        | 26.0      | 36.0 | (10.0)        | 19.0       | 14.0 | (-5.0)        |
| Grok-4-0709                | 16.2       | 2.1  | (-14.0)       | 9.0         | 2.0  | (-7.0)        | 26.0      | 29.0 | (3.0)         | 26.0       | 23.0 | (-3.0)        |
| Grok-4-Fast-Reasoning      | 6.0        | 0.0  | (-6.0)        | 3.0         | 1.0  | (-2.0)        | 29.0      | 23.0 | (-6.0)        | 22.0       | 34.0 | (12.0)        |
| <i>Open-Source MLLMs</i>   |            |      |               |             |      |               |           |      |               |            |      |               |
| Gemma-4-31B                | 63.0       | 5.0  | (-58.0)       | 26.0        | 23.0 | (-3.0)        | 39.0      | 32.0 | (-7.0)        | 41.0       | 21.0 | (-20.0)       |
| Gemma-4-26B                | 63.0       | 4.1  | (-58.9)       | 9.0         | 11.0 | (2.0)         | 26.3      | 29.0 | (2.7)         | 17.0       | 14.1 | (-2.9)        |
| Kimi-k2.5                  | 75.0       | 4.0  | (-71.0)       | 11.1        | 6.0  | (-5.1)        | 53.0      | 47.0 | (-6.0)        | 19.0       | 13.0 | (-6.0)        |
| Qwen3.5-397B-A17B          | 78.0       | 2.0  | (-76.0)       | 30.0        | 19.0 | (-11.0)       | 74.0      | 37.0 | (-37.0)       | 49.0       | 24.0 | (-25.0)       |
| Mistral-Small-2503         | 14.1       | 0.0  | (-14.1)       | 2.0         | 2.0  | (0.0)         | 27.0      | 38.0 | (11.0)        | 18.0       | 27.0 | (9.0)         |

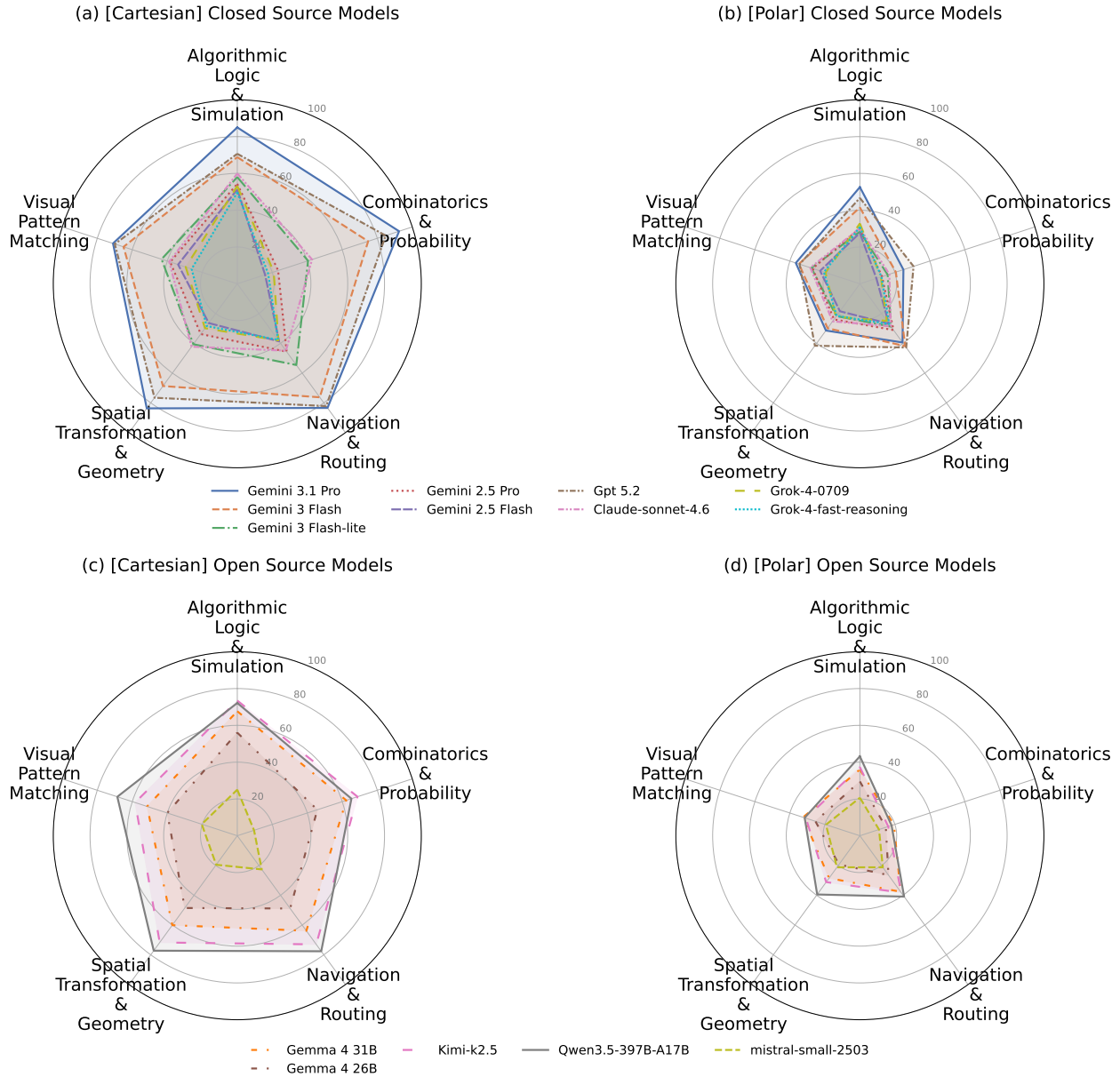


Figure 12 | Per-category radar chart comparison of all evaluated models under high reasoning mode, corresponding to Table 1. (a) Closed-source models on Cartesian layouts. (b) Closed-source models on Polar layouts. (c) Open-source models on Cartesian layouts. (d) Open-source models on Polar layouts. Each axis represents one of the five task categories, and the radial scale indicates accuracy (%).

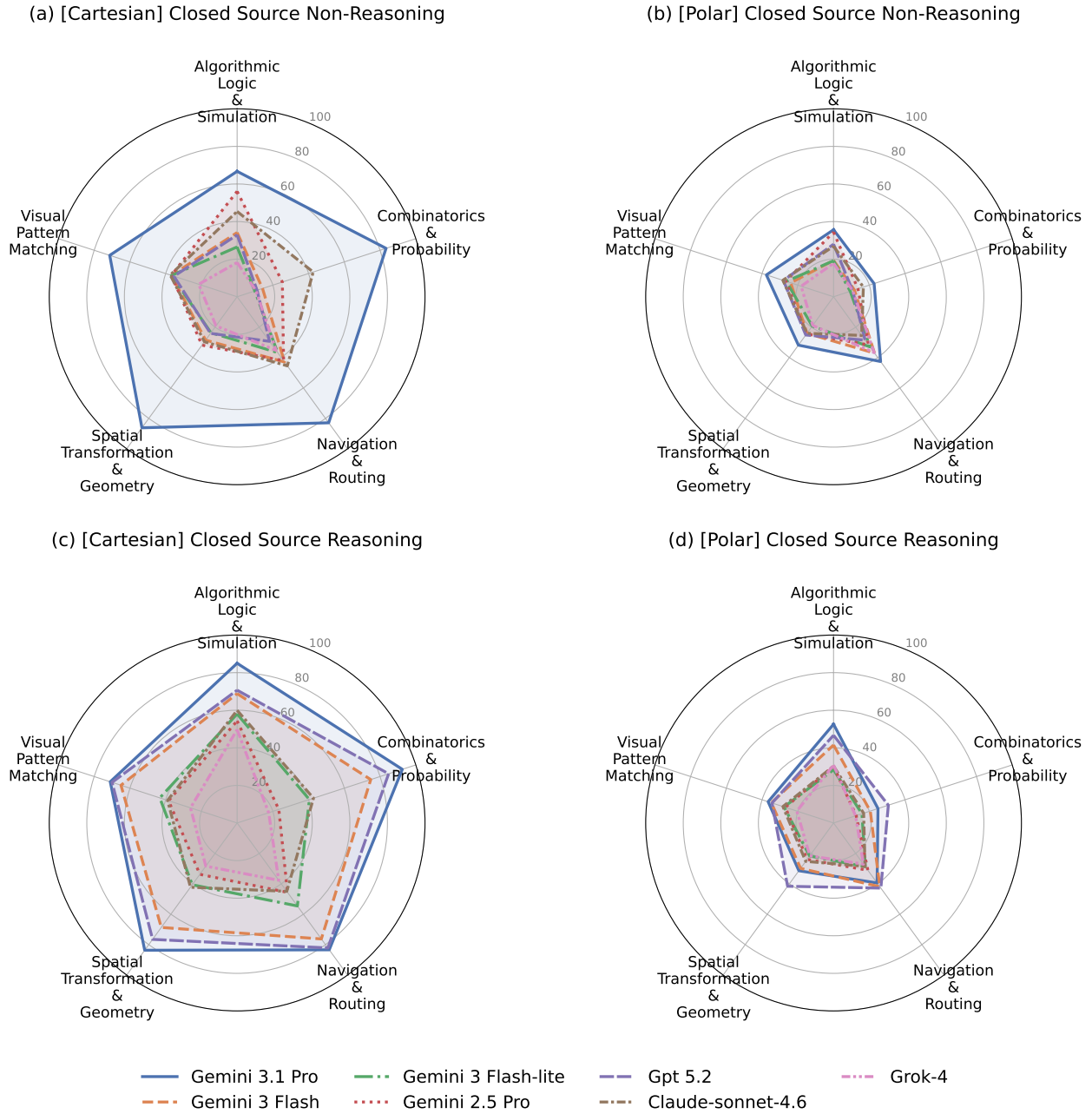


Figure 13 | Effect of reasoning mode on per-category performance for closed-source models, corresponding to Table 2. (a) Non-reasoning mode on Cartesian layouts. (b) Non-reasoning mode on Polar layouts. (c) High reasoning mode on Cartesian layouts. (d) High reasoning mode on Polar layouts.

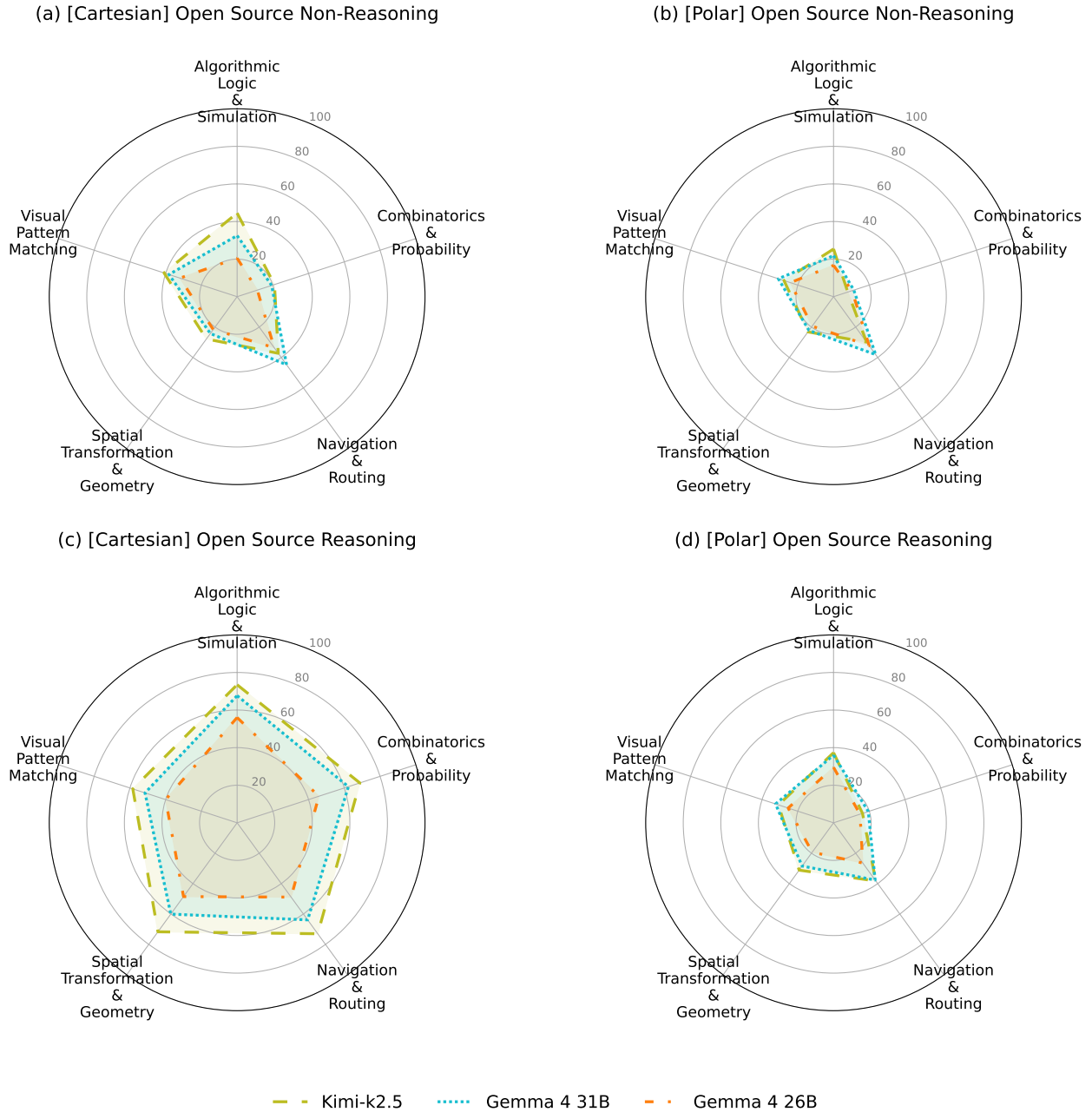


Figure 14 | Effect of reasoning mode on per-category performance for open-source models, corresponding to Table 2. (a) Non-reasoning mode on Cartesian layouts. (b) Non-reasoning mode on Polar layouts. (c) High reasoning mode on Cartesian layouts. (d) High reasoning mode on Polar layouts.

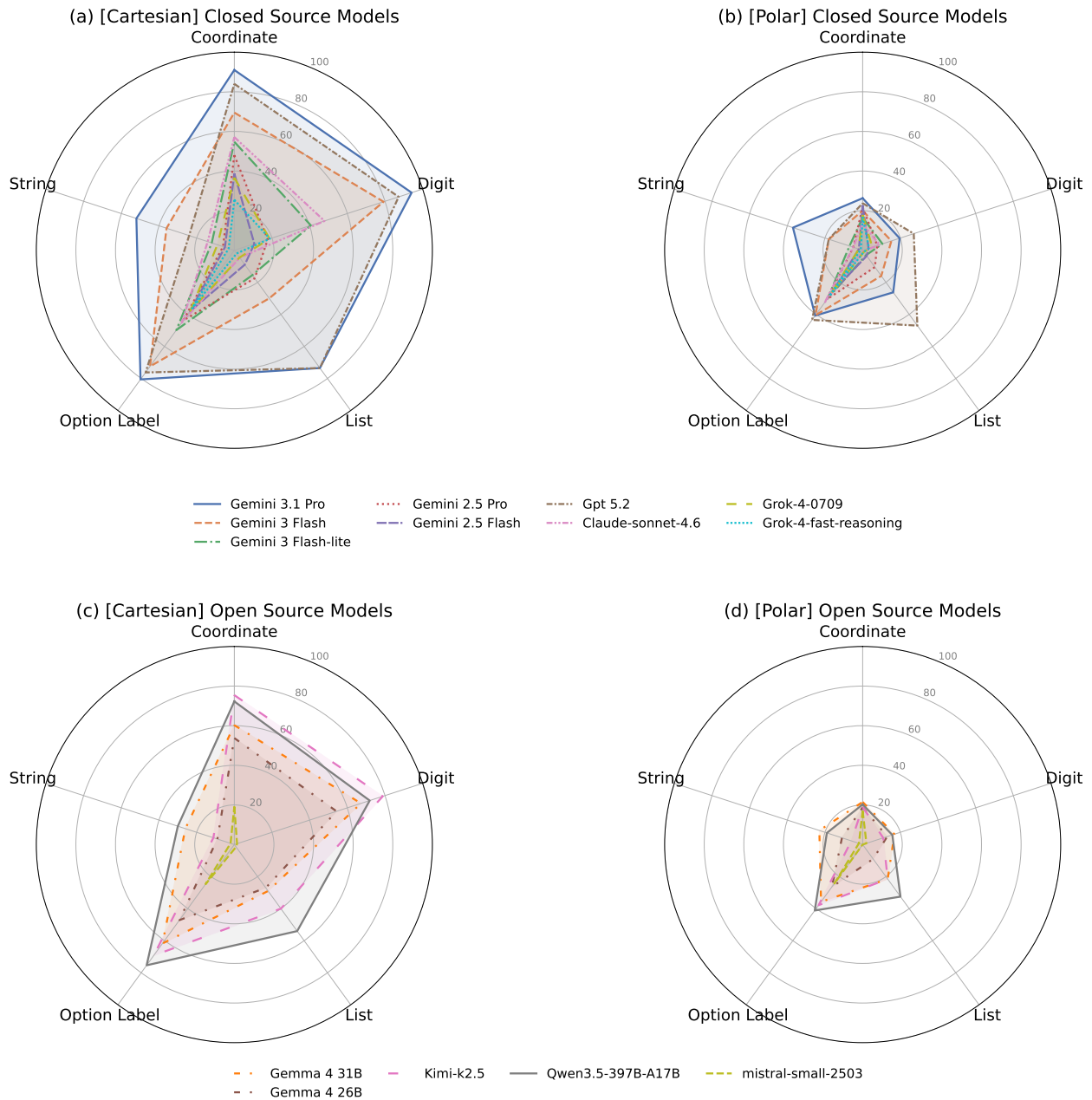


Figure 15 | Per-answer-type radar chart comparison of all evaluated models under high reasoning mode. (a) Closed-source models on Cartesian layouts. (b) Closed-source models on Polar layouts. (c) Open-source models on Cartesian layouts. (d) Open-source models on Polar layouts. Each axis represents one of the five answer types (Coordinate, Digit, String, Option Label, List), and the radial scale indicates accuracy (%).

Table 12 | Per-task results under the Visual Pattern Matching category, subcategory Shape and Jigsaw Assembly. All models are evaluated under high reasoning mode. C and P denote Cartesian and Polar accuracy (%), respectively. ( $-\Delta$ ) indicates the accuracy change from Cartesian to Polar. Task abbreviations: Frag. Match. = Fragment Matching; Jigsaw = Jigsaw Matching; Layer Comp. = Layer Completion; Pat. Comp. = Pattern Completion; Shape Comp. = Shape Completion; Shape Fit. = Shape Fitting; Tmpl. Match. = Template Matching.

| Model                      | Frag. Match. |      |               | Jigsaw |      |               | Layer Comp. |      |               | Pat. Comp. |      |               | Shape Comp. |      |               | Shape Fit. |      |               | Tmpl. Match. |      |               |
|----------------------------|--------------|------|---------------|--------|------|---------------|-------------|------|---------------|------------|------|---------------|-------------|------|---------------|------------|------|---------------|--------------|------|---------------|
|                            | C            | P    | ( $-\Delta$ ) | C      | P    | ( $-\Delta$ ) | C           | P    | ( $-\Delta$ ) | C          | P    | ( $-\Delta$ ) | C           | P    | ( $-\Delta$ ) | C          | P    | ( $-\Delta$ ) | C            | P    | ( $-\Delta$ ) |
| Random                     | 20.0         | 20.0 | (0.0)         | 20.0   | 20.0 | (0.0)         | 25.0        | 25.0 | (0.0)         | 25.0       | 25.0 | (0.0)         | 25.0        | 25.0 | (0.0)         | 33.0       | 33.0 | (0.0)         | 20.0         | 20.0 | (0.0)         |
| <i>Closed-Source MLLMs</i> |              |      |               |        |      |               |             |      |               |            |      |               |             |      |               |            |      |               |              |      |               |
| Gemini-3.1-Pro             | 59.0         | 31.0 | (-28.0)       | 80.0   | 44.0 | (-36.0)       | 93.0        | 69.7 | (-23.3)       | 55.0       | 26.0 | (-29.0)       | 43.0        | 29.3 | (-13.7)       | 60.0       | 33.0 | (-27.0)       | 97.0         | 53.5 | (-43.5)       |
| Gemini-3-Flash             | 53.0         | 25.0 | (-28.0)       | 74.0   | 50.0 | (-24.0)       | 91.0        | 70.0 | (-21.0)       | 41.0       | 20.0 | (-21.0)       | 33.0        | 22.0 | (-11.0)       | 61.0       | 45.0 | (-16.0)       | 100.0        | 62.0 | (-38.0)       |
| Gemini-3-Flash-lite        | 24.0         | 30.0 | (6.0)         | 40.0   | 34.0 | (-6.0)        | 58.0        | 47.0 | (-11.0)       | 29.0       | 19.0 | (-10.0)       | 49.0        | 29.0 | (-20.0)       | 46.0       | 34.0 | (-12.0)       | 92.0         | 37.0 | (-55.0)       |
| Gemini-2.5-Pro             | 21.0         | 19.0 | (-2.0)        | 34.0   | 34.0 | (0.0)         | 76.0        | 52.0 | (-24.0)       | 29.0       | 27.0 | (-2.0)        | 28.0        | 26.0 | (-2.0)        | 43.0       | 39.0 | (-4.0)        | 85.0         | 32.0 | (-53.0)       |
| Gemini-2.5-Flash           | 23.0         | 21.0 | (-2.0)        | 18.0   | 16.0 | (-2.0)        | 71.0        | 36.0 | (-35.0)       | 30.0       | 28.0 | (-2.0)        | 37.0        | 24.0 | (-13.0)       | 30.0       | 33.0 | (3.0)         | 76.0         | 19.0 | (-57.0)       |
| GPT-5.2                    | 95.0         | 30.0 | (-65.0)       | 54.0   | 46.0 | (-8.0)        | 88.0        | 64.0 | (-24.0)       | 94.0       | 24.0 | (-70.0)       | 52.0        | 40.0 | (-12.0)       | 48.0       | 34.0 | (-14.0)       | 100.0        | 59.0 | (-41.0)       |
| Claude-Sonnet-4.6          | 35.0         | 18.6 | (-16.5)       | 39.2   | 30.9 | (-8.2)        | 67.0        | 74.8 | (7.8)         | 31.6       | 24.0 | (-7.6)        | 41.0        | 29.3 | (-11.7)       | 49.5       | 42.4 | (-7.1)        | 31.0         | 35.7 | (4.7)         |
| Grok-4-0709                | 26.0         | 21.0 | (-5.0)        | 19.0   | 17.0 | (-2.0)        | 38.0        | 26.0 | (-12.0)       | 27.0       | 18.0 | (-9.0)        | 32.0        | 21.0 | (-11.0)       | 38.0       | 34.0 | (-4.0)        | 67.0         | 22.6 | (-44.4)       |
| Grok-4-Fast-Reasoning      | 15.0         | 17.0 | (2.0)         | 22.0   | 17.0 | (-5.0)        | 52.0        | 26.0 | (-26.0)       | 25.0       | 23.0 | (-2.0)        | 24.0        | 26.0 | (2.0)         | 38.0       | 37.0 | (-1.0)        | 51.0         | 22.0 | (-29.0)       |
| <i>Open-Source MLLMs</i>   |              |      |               |        |      |               |             |      |               |            |      |               |             |      |               |            |      |               |              |      |               |
| Gemma-4-31B                | 34.0         | 19.0 | (-15.0)       | 50.0   | 47.0 | (-3.0)        | 80.0        | 60.0 | (-20.0)       | 50.0       | 34.0 | (-16.0)       | 29.0        | 26.0 | (-3.0)        | 60.0       | 39.0 | (-21.0)       | 95.0         | 51.0 | (-44.0)       |
| Gemma-4-26B                | 31.0         | 19.0 | (-12.0)       | 34.3   | 26.0 | (-8.3)        | 64.0        | 54.0 | (-10.0)       | 29.0       | 27.0 | (-2.0)        | 22.2        | 22.2 | (0.0)         | 52.5       | 37.0 | (-15.5)       | 91.9         | 36.0 | (-55.9)       |
| Kimi-k2.5                  | 70.4         | 31.0 | (-39.4)       | 46.0   | 28.3 | (-17.7)       | 91.0        | 66.0 | (-25.0)       | 81.6       | 25.0 | (-56.6)       | 37.0        | 29.0 | (-8.0)        | 63.0       | 40.0 | (-23.0)       | 95.0         | 50.0 | (-45.0)       |
| Qwen3.5-397B-A17B          | 84.0         | 33.0 | (-51.0)       | 69.0   | 55.0 | (-14.0)       | 96.0        | 49.0 | (-47.0)       | 89.0       | 30.0 | (-59.0)       | 43.0        | 19.0 | (-24.0)       | 54.0       | 23.0 | (-31.0)       | 88.0         | 56.0 | (-32.0)       |
| Mistral-Small-2503         | 31.3         | 11.3 | (-20.0)       | 14.0   | 17.0 | (3.0)         | 7.0         | 17.0 | (10.0)        | 26.0       | 19.0 | (-7.0)        | 30.0        | 30.0 | (0.0)         | 38.0       | 33.0 | (-5.0)        | 16.0         | 19.0 | (3.0)         |

Table 13 | Per-task results under the Spatial Transformation and Geometry category, subcategory Geometric Measurement and Counting. All models are evaluated under high reasoning mode. C and P denote Cartesian and Polar accuracy (%), respectively. ( $-\Delta$ ) indicates the accuracy change from Cartesian to Polar. Task abbreviations: Area Bal. = Area Balancing; Area Cnt. = Area Counting; Curve Len. = Curve Length; Pipe Len. = Pipe Lengths.

| Model                      | Area Bal. |      |               | Area Cnt. |     |               | Curve Len. |      |               | Pipe Len. |     |               | Uncut Cells |      |               |
|----------------------------|-----------|------|---------------|-----------|-----|---------------|------------|------|---------------|-----------|-----|---------------|-------------|------|---------------|
|                            | C         | P    | ( $-\Delta$ ) | C         | P   | ( $-\Delta$ ) | C          | P    | ( $-\Delta$ ) | C         | P   | ( $-\Delta$ ) | C           | P    | ( $-\Delta$ ) |
| Random                     | 20.0      | 19.9 | (-0.1)        | 0.1       | 0.1 | (-0.0)        | 20.0       | 20.0 | (0.0)         | 0.0       | 0.0 | (0.0)         | 20.0        | 20.0 | (0.0)         |
| <i>Closed-Source MLLMs</i> |           |      |               |           |     |               |            |      |               |           |     |               |             |      |               |
| Gemini-3.1-Pro             | 66.0      | 22.0 | (-44.0)       | 94.0      | 2.0 | (-92.0)       | 69.0       | 20.0 | (-49.0)       | 75.0      | 1.0 | (-74.0)       | 89.0        | 44.0 | (-45.0)       |
| Gemini-3-Flash             | 51.0      | 22.0 | (-29.0)       | 80.0      | 4.0 | (-76.0)       | 59.0       | 39.0 | (-20.0)       | 12.0      | 2.0 | (-10.0)       | 63.0        | 41.0 | (-22.0)       |
| Gemini-3-Flash-lite        | 29.0      | 22.0 | (-7.0)        | 8.0       | 6.0 | (-2.0)        | 26.0       | 26.0 | (0.0)         | 4.0       | 0.0 | (-4.0)        | 40.0        | 35.0 | (-5.0)        |
| Gemini-2.5-Pro             | 20.0      | 18.0 | (-2.0)        | 6.0       | 4.0 | (-2.0)        | 38.0       | 40.0 | (2.0)         | 1.0       | 1.0 | (0.0)         | 45.0        | 34.0 | (-11.0)       |
| Gemini-2.5-Flash           | 23.0      | 16.0 | (-7.0)        | 1.0       | 2.0 | (1.0)         | 23.0       | 15.0 | (-8.0)        | 0.0       | 2.0 | (2.0)         | 34.0        | 28.0 | (-6.0)        |
| GPT-5.2                    | 46.0      | 21.0 | (-25.0)       | 88.0      | 7.0 | (-81.0)       | 35.0       | 29.0 | (-6.0)        | 56.0      | 7.0 | (-49.0)       | 50.0        | 41.0 | (-9.0)        |
| Claude-Sonnet-4.6          | 18.2      | 10.0 | (-8.2)        | 37.4      | 1.0 | (-36.4)       | 75.8       | 87.6 | (11.8)        | 2.0       | 0.0 | (-2.0)        | 43.3        | 47.4 | (4.1)         |
| Grok-4-0709                | 20.0      | 20.0 | (0.0)         | 0.0       | 2.0 | (2.0)         | 60.0       | 67.0 | (7.0)         | 0.0       | 0.0 | (0.0)         | 34.7        | 36.4 | (1.7)         |
| Grok-4-Fast-Reasoning      | 17.0      | 13.0 | (-4.0)        | 1.0       | 0.0 | (-1.0)        | 94.0       | 90.0 | (-4.0)        | 0.0       | 0.0 | (0.0)         | 38.0        | 43.0 | (5.0)         |
| <i>Open-Source MLLMs</i>   |           |      |               |           |     |               |            |      |               |           |     |               |             |      |               |
| Gemma-4-31B                | 48.0      | 24.0 | (-24.0)       | 53.0      | 6.0 | (-47.0)       | 46.0       | 25.0 | (-21.0)       | 1.0       | 0.0 | (-1.0)        | 62.0        | 41.0 | (-21.0)       |
| Gemma-4-26B                | 20.0      | 22.0 | (2.0)         | 40.0      | 5.0 | (-35.0)       | 9.1        | 5.0  | (-4.0)        | 11.0      | 0.0 | (-11.0)       | 52.0        | 20.2 | (-31.8)       |
| Kimi-k2.5                  | 46.0      | 22.4 | (-23.6)       | 98.0      | 3.0 | (-95.0)       | 52.0       | 70.7 | (18.7)        | 12.0      | 1.0 | (-11.0)       | 58.6        | 36.0 | (-22.6)       |
| Qwen3.5-397B-A17B          | 52.0      | 20.0 | (-32.0)       | 72.0      | 7.0 | (-65.0)       | 47.0       | 32.0 | (-15.0)       | 27.0      | 3.0 | (-24.0)       | 75.0        | 32.0 | (-43.0)       |
| Mistral-Small-2503         | 20.0      | 27.0 | (7.0)         | 0.0       | 0.0 | (0.0)         | 54.7       | 74.0 | (19.3)        | 0.0       | 0.0 | (0.0)         | 19.0        | 17.0 | (-2.0)        |

Table 14 | Per-task results under the Spatial Transformation and Geometry category, subcategory Spatial Constraints and Topology. All models are evaluated under high reasoning mode. C and P denote Cartesian and Polar accuracy (%), respectively.  $(-\Delta)$  indicates the accuracy change from Cartesian to Polar. Task abbreviations: Grid Fold. = Grid Folding; Imp. Shape = Impossible Shape.

| Model                      | Four Color |      |             | Grid Fold. |      |             | Imp. Shape |      |             |
|----------------------------|------------|------|-------------|------------|------|-------------|------------|------|-------------|
|                            | C          | P    | $(-\Delta)$ | C          | P    | $(-\Delta)$ | C          | P    | $(-\Delta)$ |
| Random                     | 20.0       | 20.0 | (0.0)       | 20.0       | 20.0 | (0.0)       | 20.0       | 20.0 | (0.0)       |
| <i>Closed-Source MLLMs</i> |            |      |             |            |      |             |            |      |             |
| Gemini-3.1-Pro             | 91.9       | 28.3 | (-63.6)     | 100.0      | 54.1 | (-45.9)     | 62.0       | 20.0 | (-42.0)     |
| Gemini-3-Flash             | 86.0       | 19.0 | (-67.0)     | 99.0       | 47.0 | (-52.0)     | 41.0       | 20.0 | (-21.0)     |
| Gemini-3-Flash-lite        | 44.0       | 18.0 | (-26.0)     | 86.0       | 41.0 | (-45.0)     | 28.0       | 22.0 | (-6.0)      |
| Gemini-2.5-Pro             | 30.0       | 20.0 | (-10.0)     | 60.0       | 42.0 | (-18.0)     | 14.0       | 10.0 | (-4.0)      |
| Gemini-2.5-Flash           | 24.0       | 25.0 | (1.0)       | 40.0       | 26.0 | (-14.0)     | 23.0       | 22.0 | (-1.0)      |
| GPT-5.2                    | 98.0       | 27.0 | (-71.0)     | 100.0      | 59.0 | (-41.0)     | 43.0       | 22.0 | (-21.0)     |
| Claude-Sonnet-4.6          | 45.4       | 19.2 | (-26.2)     | 100.0      | 37.1 | (-62.9)     | 19.2       | 17.2 | (-2.0)      |
| Grok-4-0709                | 34.0       | 25.0 | (-9.0)      | 45.0       | 23.0 | (-22.0)     | 24.0       | 24.0 | (0.0)       |
| Grok-4-Fast-Reasoning      | 28.0       | 28.0 | (0.0)       | 51.0       | 18.0 | (-33.0)     | 21.0       | 15.0 | (-6.0)      |
| <i>Open-Source MLLMs</i>   |            |      |             |            |      |             |            |      |             |
| Gemma-4-31B                | 65.0       | 32.0 | (-33.0)     | 97.0       | 44.0 | (-53.0)     | 33.0       | 22.0 | (-11.0)     |
| Gemma-4-26B                | 51.5       | 19.0 | (-32.5)     | 98.0       | 36.0 | (-62.0)     | 25.5       | 13.0 | (-12.5)     |
| Kimi-k2.5                  | 81.8       | 26.0 | (-55.8)     | 99.0       | 39.0 | (-60.0)     | 56.0       | 13.0 | (-43.0)     |
| Qwen3.5-397B-A17B          | 92.0       | 43.0 | (-49.0)     | 100.0      | 64.0 | (-36.0)     | 82.0       | 26.0 | (-56.0)     |
| Mistral-Small-2503         | 18.2       | 17.0 | (-1.2)      | 20.0       | 21.2 | (1.2)       | 18.6       | 28.3 | (9.7)       |

Table 15 | Per-task results under the Spatial Transformation and Geometry category, subcategory Rotations and Reflections. All models are evaluated under high reasoning mode. C and P denote Cartesian and Polar accuracy (%), respectively.  $(-\Delta)$  indicates the accuracy change from Cartesian to Polar. Task abbreviations: Grid Rot. = Grid Rotation; Mirror Ref. = Mirror Reflection; Pivot Rot. = Pivot Rotation; Rot. Center = Rotation Center; Rot. Match. = Rotation Matching.

| Model                      | Grid Rot. |      |             | Mirror Ref. |      |             | Pivot Rot. |      |             | Rot. Center |      |             | Rot. Match. |      |             |
|----------------------------|-----------|------|-------------|-------------|------|-------------|------------|------|-------------|-------------|------|-------------|-------------|------|-------------|
|                            | C         | P    | $(-\Delta)$ | C           | P    | $(-\Delta)$ | C          | P    | $(-\Delta)$ | C           | P    | $(-\Delta)$ | C           | P    | $(-\Delta)$ |
| Random                     | 20.0      | 20.0 | (0.0)       | 25.0        | 25.0 | (0.0)       | 20.0       | 20.0 | (0.0)       | 25.0        | 25.0 | (0.0)       | 0.0         | 0.0  | (0.0)       |
| <i>Closed-Source MLLMs</i> |           |      |             |             |      |             |            |      |             |             |      |             |             |      |             |
| Gemini-3.1-Pro             | 98.0      | 31.0 | (-67.0)     | 84.0        | 42.0 | (-42.0)     | 87.0       | 51.5 | (-35.5)     | 100.0       | 40.8 | (-59.2)     | 72.0        | 51.5 | (-20.5)     |
| Gemini-3-Flash             | 99.0      | 35.0 | (-64.0)     | 76.0        | 47.0 | (-29.0)     | 83.0       | 62.0 | (-21.0)     | 96.0        | 20.0 | (-76.0)     | 48.0        | 30.0 | (-18.0)     |
| Gemini-3-Flash-lite        | 73.0      | 23.0 | (-50.0)     | 33.0        | 36.0 | (3.0)       | 52.0       | 36.0 | (-16.0)     | 78.0        | 11.0 | (-67.0)     | 27.0        | 6.0  | (-21.0)     |
| Gemini-2.5-Pro             | 30.0      | 20.0 | (-10.0)     | 38.0        | 35.0 | (-3.0)      | 48.0       | 33.0 | (-15.0)     | 75.0        | 34.0 | (-41.0)     | 34.0        | 20.0 | (-14.0)     |
| Gemini-2.5-Flash           | 27.0      | 23.0 | (-4.0)      | 32.0        | 27.0 | (-5.0)      | 32.0       | 22.0 | (-10.0)     | 66.0        | 27.0 | (-39.0)     | 18.0        | 5.0  | (-13.0)     |
| GPT-5.2                    | 100.0     | 87.0 | (-13.0)     | 98.0        | 58.0 | (-40.0)     | 94.0       | 68.0 | (-26.0)     | 96.0        | 28.0 | (-68.0)     | 91.0        | 87.0 | (-4.0)      |
| Claude-Sonnet-4.6          | 53.1      | 19.2 | (-33.9)     | 39.0        | 43.0 | (4.0)       | 40.0       | 32.0 | (-8.0)      | 68.7        | 13.3 | (-55.4)     | 7.2         | 1.0  | (-6.2)      |
| Grok-4-0709                | 34.0      | 21.0 | (-13.0)     | 35.0        | 32.0 | (-3.0)      | 33.0       | 21.2 | (-11.8)     | 59.6        | 15.0 | (-44.6)     | 9.0         | 2.0  | (-7.0)      |
| Grok-4-Fast-Reasoning      | 21.0      | 18.0 | (-3.0)      | 25.0        | 25.0 | (0.0)       | 28.0       | 13.0 | (-15.0)     | 41.0        | 15.0 | (-26.0)     | 4.0         | 2.0  | (-2.0)      |
| <i>Open-Source MLLMs</i>   |           |      |             |             |      |             |            |      |             |             |      |             |             |      |             |
| Gemma-4-31B                | 97.0      | 28.0 | (-69.0)     | 64.0        | 35.0 | (-29.0)     | 76.0       | 44.0 | (-32.0)     | 82.0        | 26.0 | (-56.0)     | 57.0        | 43.0 | (-14.0)     |
| Gemma-4-26B                | 92.0      | 25.2 | (-66.8)     | 62.0        | 40.0 | (-22.0)     | 57.0       | 42.0 | (-15.0)     | 70.0        | 6.1  | (-63.9)     | 43.0        | 18.0 | (-25.0)     |
| Kimi-k2.5                  | 100.0     | 29.0 | (-71.0)     | 91.9        | 53.5 | (-38.4)     | 78.0       | 52.5 | (-25.5)     | 90.7        | 16.7 | (-74.0)     | 68.0        | 42.0 | (-26.0)     |
| Qwen3.5-397B-A17B          | 100.0     | 73.0 | (-27.0)     | 94.0        | 56.0 | (-38.0)     | 89.0       | 60.0 | (-29.0)     | 93.0        | 35.0 | (-58.0)     | 81.0        | 62.0 | (-19.0)     |
| Mistral-Small-2503         | 23.0      | 15.3 | (-7.7)      | 27.0        | 34.0 | (7.0)       | 13.0       | 20.0 | (7.0)       | 37.0        | 22.0 | (-15.0)     | 3.0         | 0.0  | (-3.0)      |

Table 16 | Per-task results under the Algorithmic Logic and Simulation category. All models are evaluated under high reasoning mode. C and P denote Cartesian and Polar accuracy (%), respectively.  $(-\Delta)$  indicates the accuracy change from Cartesian to Polar. Task abbreviations: Bounce = Bouncing Point; Collision = Collision Detection; Max. Coll. = Maximum Collection; Min. Flips = Minimum Flips.

| Model                      | Bounce |      |             | Collision |      |             | Max. Coll. |      |             | Min. Flips |      |             | N-Queens |      |             | Sudoku |      |             |
|----------------------------|--------|------|-------------|-----------|------|-------------|------------|------|-------------|------------|------|-------------|----------|------|-------------|--------|------|-------------|
|                            | C      | P    | $(-\Delta)$ | C         | P    | $(-\Delta)$ | C          | P    | $(-\Delta)$ | C          | P    | $(-\Delta)$ | C        | P    | $(-\Delta)$ | C      | P    | $(-\Delta)$ |
| Random                     | 1.8    | 1.8  | (-0.0)      | 20.0      | 20.0 | (0.0)       | 20.0       | 20.0 | (0.0)       | 20.0       | 20.0 | (0.0)       | 20.0     | 20.0 | (0.0)       | 20.0   | 20.0 | (0.0)       |
| <i>Closed-Source MLLMs</i> |        |      |             |           |      |             |            |      |             |            |      |             |          |      |             |        |      |             |
| Gemini-3.1-Pro             | 97.0   | 30.6 | (-66.4)     | 58.0      | 34.0 | (-24.0)     | 66.0       | 31.0 | (-35.0)     | 88.9       | 85.7 | (-3.2)      | 100.0    | 74.0 | (-26.0)     | 100.0  | 60.0 | (-40.0)     |
| Gemini-3-Flash             | 49.0   | 28.0 | (-21.0)     | 67.0      | 31.0 | (-36.0)     | 30.0       | 20.0 | (-10.0)     | 68.0       | 53.0 | (-15.0)     | 100.0    | 50.0 | (-50.0)     | 99.0   | 67.0 | (-32.0)     |
| Gemini-3-Flash-lite        | 34.0   | 16.0 | (-18.0)     | 54.0      | 27.0 | (-27.0)     | 27.0       | 18.0 | (-9.0)      | 37.0       | 32.0 | (-5.0)      | 100.0    | 33.0 | (-67.0)     | 96.0   | 44.0 | (-52.0)     |
| Gemini-2.5-Pro             | 32.0   | 25.0 | (-7.0)      | 48.0      | 29.0 | (-19.0)     | 18.0       | 17.0 | (-1.0)      | 36.0       | 24.0 | (-12.0)     | 99.0     | 34.0 | (-65.0)     | 93.0   | 52.0 | (-41.0)     |
| Gemini-2.5-Flash           | 19.0   | 24.0 | (5.0)       | 46.0      | 25.0 | (-21.0)     | 20.0       | 14.0 | (-6.0)      | 31.0       | 31.0 | (0.0)       | 99.0     | 35.0 | (-64.0)     | 93.0   | 37.0 | (-56.0)     |
| GPT-5.2                    | 79.0   | 32.0 | (-47.0)     | 61.0      | 40.0 | (-21.0)     | 43.0       | 17.0 | (-26.0)     | 41.0       | 30.0 | (-11.0)     | 100.0    | 90.0 | (-10.0)     | 100.0  | 71.0 | (-29.0)     |
| Claude-Sonnet-4.6          | 86.3   | 9.6  | (-76.8)     | 51.0      | 32.3 | (-18.7)     | 20.6       | 33.3 | (12.7)      | 18.9       | 22.7 | (3.7)       | 99.0     | 34.7 | (-64.2)     | 83.8   | 49.0 | (-34.8)     |
| Grok-4-0709                | 21.9   | 17.2 | (-4.7)      | 38.4      | 29.0 | (-9.4)      | 26.0       | 29.3 | (3.3)       | 55.7       | 56.1 | (0.5)       | 96.0     | 29.0 | (-67.0)     | 81.0   | 36.0 | (-45.0)     |
| Grok-4-Fast-Reasoning      | 17.0   | 13.0 | (-4.0)      | 30.0      | 25.0 | (-5.0)      | 34.0       | 30.0 | (-4.0)      | 57.0       | 55.0 | (-2.0)      | 76.0     | 26.0 | (-50.0)     | 84.0   | 36.0 | (-48.0)     |
| <i>Open-Source MLLMs</i>   |        |      |             |           |      |             |            |      |             |            |      |             |          |      |             |        |      |             |
| Gemma-4-31B                | 48.0   | 21.0 | (-27.0)     | 53.0      | 26.0 | (-27.0)     | 52.0       | 27.0 | (-25.0)     | 55.0       | 36.0 | (-19.0)     | 100.0    | 56.0 | (-44.0)     | 98.0   | 50.0 | (-48.0)     |
| Gemma-4-26B                | 42.0   | 23.0 | (-19.0)     | 39.0      | 14.0 | (-25.0)     | 14.1       | 8.0  | (-6.1)      | 43.0       | 36.0 | (-7.0)      | 100.0    | 46.0 | (-54.0)     | 98.0   | 50.0 | (-48.0)     |
| Kimi-k2.5                  | 90.6   | 17.8 | (-72.8)     | 56.0      | 32.0 | (-24.0)     | 36.8       | 22.3 | (-14.5)     | 59.4       | 45.2 | (-14.2)     | 99.0     | 53.7 | (-45.3)     | 99.0   | 53.0 | (-46.0)     |
| Qwen3.5-397B-A17B          | 58.0   | 25.0 | (-33.0)     | 58.0      | 37.0 | (-21.0)     | 70.0       | 29.0 | (-41.0)     | 56.0       | 51.0 | (-5.0)      | 100.0    | 46.0 | (-54.0)     | 91.0   | 71.0 | (-20.0)     |
| Mistral-Small-2503         | 4.5    | 0.0  | (-4.5)      | 31.0      | 35.7 | (4.7)       | 22.0       | 18.0 | (-4.0)      | 15.8       | 24.2 | (8.4)       | 38.0     | 20.0 | (-18.0)     | 39.0   | 26.0 | (-13.0)     |

Table 17 | Per-task results under the Combinatorics and Probability category, subcategory Bounded Combinatorics. All models are evaluated under high reasoning mode. C and P denote Cartesian and Polar accuracy (%), respectively.  $(-\Delta)$  indicates the accuracy change from Cartesian to Polar. Task abbreviations: Bnd. Diag. = Bounded Diagonal Paths; Bnd. Knight = Bounded Knight Paths; Chkpt. Path = Checkpoint Paths; Lattice = Lattice Paths; Path Cnt. = Path Counting.

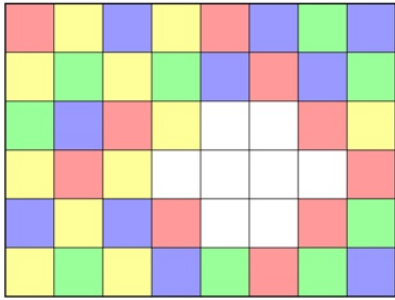
| Model                      | Bnd. Diag. |      |             | Bnd. Knight |      |             | Chkpt. Path |      |             | Lattice |      |             | Path Cnt. |      |             |
|----------------------------|------------|------|-------------|-------------|------|-------------|-------------|------|-------------|---------|------|-------------|-----------|------|-------------|
|                            | C          | P    | $(-\Delta)$ | C           | P    | $(-\Delta)$ | C           | P    | $(-\Delta)$ | C       | P    | $(-\Delta)$ | C         | P    | $(-\Delta)$ |
| Random                     | 0.0        | 0.0  | (0.0)       | 0.0         | 0.0  | (0.0)       | 0.0         | 0.0  | (0.0)       | 0.0     | 0.0  | (0.0)       | 20.0      | 20.0 | (0.0)       |
| <i>Closed-Source MLLMs</i> |            |      |             |             |      |             |             |      |             |         |      |             |           |      |             |
| Gemini-3.1-Pro             | 100.0      | 64.3 | (-35.7)     | 92.0        | 4.0  | (-88.0)     | 99.0        | 10.0 | (-89.0)     | 88.0    | 19.0 | (-69.0)     | 82.0      | 23.0 | (-59.0)     |
| Gemini-3-Flash             | 97.0       | 39.0 | (-58.0)     | 76.0        | 6.0  | (-70.0)     | 81.0        | 5.0  | (-76.0)     | 76.0    | 13.0 | (-63.0)     | 59.0      | 34.0 | (-25.0)     |
| Gemini-3-Flash-lite        | 53.0       | 42.0 | (-11.0)     | 23.0        | 1.0  | (-22.0)     | 55.0        | 1.0  | (-54.0)     | 40.0    | 4.0  | (-36.0)     | 38.0      | 27.0 | (-11.0)     |
| Gemini-2.5-Pro             | 29.0       | 23.0 | (-6.0)      | 4.0         | 0.0  | (-4.0)      | 25.0        | 1.0  | (-24.0)     | 9.0     | 2.0  | (-7.0)      | 32.0      | 28.0 | (-4.0)      |
| Gemini-2.5-Flash           | 12.0       | 11.0 | (-1.0)      | 1.0         | 1.0  | (0.0)       | 9.0         | 0.0  | (-9.0)      | 6.0     | 1.0  | (-5.0)      | 20.0      | 18.0 | (-2.0)      |
| GPT-5.2                    | 98.0       | 78.0 | (-20.0)     | 88.0        | 33.0 | (-55.0)     | 71.0        | 0.0  | (-71.0)     | 83.0    | 9.0  | (-74.0)     | 85.0      | 22.0 | (-63.0)     |
| Claude-Sonnet-4.6          | 74.7       | 38.0 | (-36.7)     | 66.7        | 9.5  | (-57.2)     | 62.5        | 4.3  | (-58.2)     | 29.4    | 3.1  | (-26.2)     | 27.6      | 32.0 | (4.5)       |
| Grok-4-0709                | 17.2       | 13.0 | (-4.1)      | 4.5         | 1.0  | (-3.5)      | 7.3         | 0.0  | (-7.3)      | 10.0    | 2.0  | (-8.0)      | 28.0      | 25.0 | (-3.0)      |
| Grok-4-Fast-Reasoning      | 27.0       | 13.0 | (-14.0)     | 9.0         | 0.0  | (-9.0)      | 5.0         | 0.0  | (-5.0)      | 2.0     | 2.0  | (0.0)       | 31.0      | 32.0 | (1.0)       |
| <i>Open-Source MLLMs</i>   |            |      |             |             |      |             |             |      |             |         |      |             |           |      |             |
| Gemma-4-31B                | 91.0       | 52.0 | (-39.0)     | 56.0        | 8.0  | (-48.0)     | 48.0        | 7.0  | (-41.0)     | 75.0    | 7.0  | (-68.0)     | 41.0      | 22.0 | (-19.0)     |
| Gemma-4-26B                | 80.0       | 50.0 | (-30.0)     | 51.0        | 4.1  | (-46.9)     | 22.0        | 5.0  | (-17.0)     | 48.0    | 9.0  | (-39.0)     | 10.2      | 11.2 | (1.0)       |
| Kimi-k2.5                  | 96.9       | 16.7 | (-80.2)     | 79.4        | 4.1  | (-75.3)     | 51.6        | 1.1  | (-50.6)     | 52.0    | 5.0  | (-47.0)     | 49.0      | 27.6 | (-21.4)     |
| Qwen3.5-397B-A17B          | 99.0       | 35.0 | (-64.0)     | 41.0        | 9.0  | (-32.0)     | 81.0        | 4.0  | (-77.0)     | 77.0    | 6.0  | (-71.0)     | 8.0       | 4.0  | (-4.0)      |
| Mistral-Small-2503         | 0.0        | 0.0  | (0.0)       | 2.1         | 1.0  | (-1.1)      | 3.5         | 0.0  | (-3.5)      | 0.0     | 1.0  | (1.0)       | 23.0      | 27.0 | (4.0)       |

Table 18 | Per-task results under the Combinatorics and Probability category, subcategories Stochastic Processes and Topological Combinatorics. All models are evaluated under high reasoning mode. C and P denote Cartesian and Polar accuracy (%), respectively. ( $-\Delta$ ) indicates the accuracy change from Cartesian to Polar. Task abbreviations: Edge Cnt. = Edge Counting; Rand. Walk = Random Walk; Knight Path = Knight Paths; Wrap. Diag. = Wrapping Diagonal Paths.

| Model                      | Edge Cnt. |      |               | Rand. Walk |      |               | Knight Path |      |               | Wrap. Diag. |      |               |
|----------------------------|-----------|------|---------------|------------|------|---------------|-------------|------|---------------|-------------|------|---------------|
|                            | C         | P    | ( $-\Delta$ ) | C          | P    | ( $-\Delta$ ) | C           | P    | ( $-\Delta$ ) | C           | P    | ( $-\Delta$ ) |
| Random                     | 20.0      | 20.0 | (0.0)         | 20.0       | 20.0 | (0.0)         | 0.0         | 0.0  | (0.0)         | 0.0         | 0.0  | (0.0)         |
| <i>Closed-Source MLLMs</i> |           |      |               |            |      |               |             |      |               |             |      |               |
| Gemini-3.1-Pro             | 91.0      | 25.0 | (-66.0)       | 100.0      | 40.8 | (-59.2)       | 90.0        | 2.0  | (-88.0)       | 90.0        | 35.7 | (-54.3)       |
| Gemini-3-Flash             | 65.0      | 34.0 | (-31.0)       | 93.0       | 26.0 | (-67.0)       | 74.0        | 5.0  | (-69.0)       | 52.0        | 23.0 | (-29.0)       |
| Gemini-3-Flash-lite        | 28.0      | 29.0 | (1.0)         | 78.0       | 23.0 | (-55.0)       | 28.0        | 1.0  | (-27.0)       | 21.0        | 15.0 | (-6.0)        |
| Gemini-2.5-Pro             | 29.0      | 27.0 | (-2.0)        | 66.0       | 24.0 | (-42.0)       | 3.0         | 1.0  | (-2.0)        | 13.0        | 8.0  | (-5.0)        |
| Gemini-2.5-Flash           | 21.0      | 26.0 | (5.0)         | 68.0       | 25.0 | (-43.0)       | 2.0         | 2.0  | (0.0)         | 4.0         | 1.0  | (-3.0)        |
| GPT-5.2                    | 67.0      | 36.0 | (-31.0)       | 99.0       | 44.0 | (-55.0)       | 88.0        | 28.0 | (-60.0)       | 84.0        | 26.0 | (-58.0)       |
| Claude-Sonnet-4.6          | 40.4      | 39.4 | (-1.0)        | 42.5       | 23.2 | (-19.4)       | 18.8        | 0.0  | (-18.8)       | 22.1        | 2.1  | (-20.0)       |
| Grok-4-0709                | 39.0      | 40.0 | (1.0)         | 62.2       | 17.2 | (-45.0)       | 5.2         | 1.0  | (-4.2)        | 14.0        | 9.0  | (-5.0)        |
| Grok-4-Fast-Reasoning      | 41.0      | 36.0 | (-5.0)        | 26.0       | 20.0 | (-6.0)        | 7.0         | 0.0  | (-7.0)        | 11.0        | 8.0  | (-3.0)        |
| <i>Open-Source MLLMs</i>   |           |      |               |            |      |               |             |      |               |             |      |               |
| Gemma-4-31B                | 41.4      | 18.0 | (-23.4)       | 89.0       | 45.0 | (-44.0)       | 66.0        | 7.0  | (-59.0)       | 53.0        | 9.0  | (-44.0)       |
| Gemma-4-26B                | 22.2      | 14.0 | (-8.2)        | 83.0       | 23.0 | (-60.0)       | 62.0        | 4.0  | (-58.0)       | 33.3        | 13.0 | (-20.3)       |
| Kimi-k2.5                  | 41.0      | 34.0 | (-7.0)        | 92.6       | 43.3 | (-49.3)       | 85.6        | 7.1  | (-78.5)       | 70.0        | 7.0  | (-63.0)       |
| Qwen3.5-397B-A17B          | 68.0      | 31.0 | (-37.0)       | 96.0       | 49.0 | (-47.0)       | 53.0        | 6.0  | (-47.0)       | 64.0        | 19.0 | (-45.0)       |
| Mistral-Small-2503         | 38.5      | 41.2 | (2.7)         | 18.0       | 26.0 | (8.0)         | 0.0         | 2.0  | (2.0)         | 1.0         | 0.0  | (-1.0)        |

**Four Color**

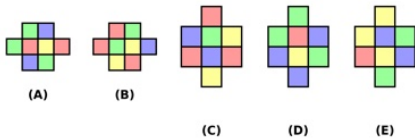
**Cartesian**



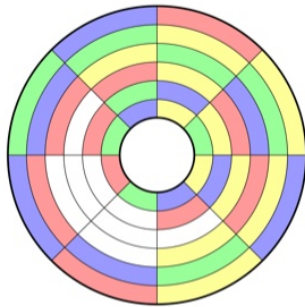
In the diagram below, two neighbouring cells are never allowed to have the same color. Which puzzle piece has to be placed in the gap so that this rule is followed? Note: You can rotate the pieces.

(A) (B) (C) (D) (E)

**Answer: E**



**Polar**



In the diagram below, two neighbouring cells are never allowed to have the same color. Which puzzle piece has to be placed in the gap so that this rule is followed? Note: You can rotate the pieces.

(A) (B) (C) (D) (E)

**Answer: E**

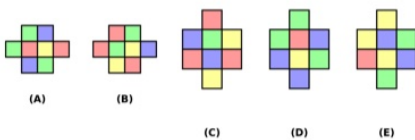
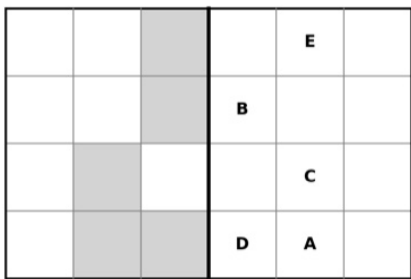


Figure 16 | Caption

**Grid Folding**

**Cartesian**

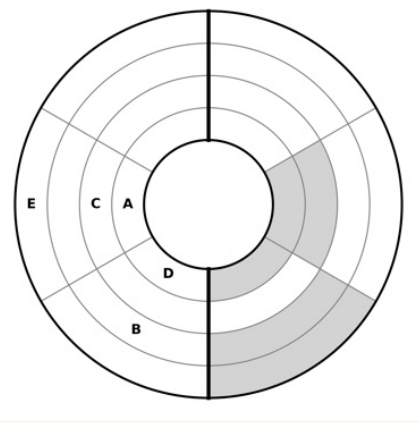


A page is folded along the thick line as shown. Which letter will NOT be covered by a grey square?

- (A) (B) (C) (D) (E)

**Answer: E**

**Polar**



A page is folded along the thick line as shown. Which letter will NOT be covered by a grey cell?

- (A) (B) (C) (D) (E)

**Answer: E**

Figure 17 | Caption







**Sudoku**

**Cartesian**

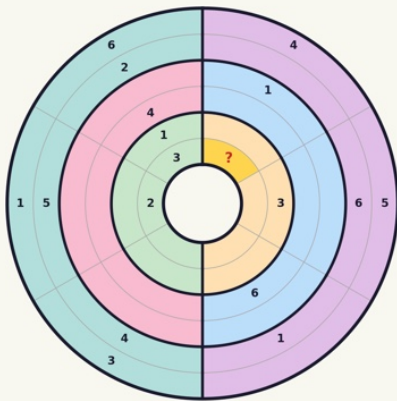
|   |   |   |   |   |
|---|---|---|---|---|
| ? |   |   | 2 | 3 |
|   | 3 |   |   | 1 |
| 1 |   | 6 |   | 4 |
|   | 6 | 1 | 4 | 5 |
| 4 | 5 |   | 3 | 1 |
|   |   |   | 2 | 6 |

In this 6x6 Sudoku puzzle, each row, each column, and each outlined box must contain all numbers from 1 to 6 exactly once. Rows are numbered 1 to 6 from top to bottom, and columns are numbered 1 to 6 from left to right. What number should replace the '?' in the highlighted cell (row 1, column 1)?

- (A) 1 (B) 2 (C) 3 (D) 5 (E) 6

**Answer: E**

**Polar**



In this polar Sudoku puzzle (6 rings — 6 sectors), each ring, each sector, and each outlined region must contain all numbers from 1 to 6 exactly once. The rings are numbered 1 to 6 from the innermost to the outermost ring. The sectors are numbered 1 to 6 clockwise starting from the top (12 o'clock).

What number should replace the '?' in the highlighted cell (ring 1, sector 1)?

- (A) 1 (B) 2 (C) 3 (D) 5 (E) 6

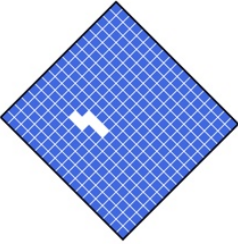
**Answer: E**

Figure 21 | Example from sudoku task.




### Shape Fitting

**Cartesian**

Complete the image



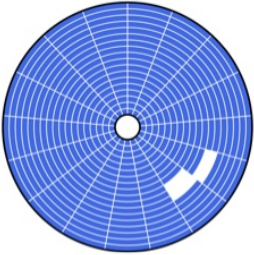
Option A      Option B      Option C






Choose the appropriate option to fill in the blank, so that the image is complete.  
A B C  
**Answer: B**

**Polar**

Complete the image



Option A      Option B      Option C



Choose the appropriate option to fill in the blank, so that the image is complete.  
A B C  
**Answer: B**

Figure 22 | Example from shape fitting task.

## Word Search

### Cartesian

|   |   |   |   |   |   |   |
|---|---|---|---|---|---|---|
| B | A | V | D | N | T | D |
| D | E | D | V | Y | E | I |
| F | D | S | I | N | D | Y |
| D | N | G | W | I | N | D |
| X | D | N | I | X | M | J |
| U | M | R | N | D | V | S |
| M | K | S | D | I | X | A |

In the grid of characters below, by how many different paths can one spell 'WIND'? Beginning at the 'W' in the middle, a path allows only moves from one cell to an adjacent (above, below, left, or right) cell.

**Answer: 7**

### Octagonal



In the octagonal grid below, by how many different paths can one spell 'WIND'? Beginning at the 'W' in the middle, a path allows only moves from one cell to an adjacent cell through the light open boundaries (up, down, left, right), without crossing the thick dark diagonal walls.

**Answer: 7**

### Hexagonal



In the honeycomb grid below, by how many different paths can one spell 'WIND'? Beginning at the 'W' in the middle, a path allows only moves from one cell to an adjacent cell through the light open boundaries, without crossing the thick dark walls.

**Answer: 7**

### Polar (Graph)



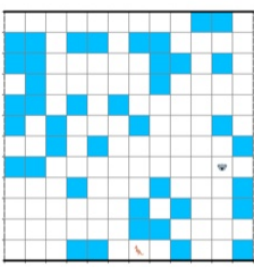
In the node-link graph below, by how many different paths can one spell 'WIND'? Beginning at the 'W' in the center node, a path allows only moves from one node to an adjacent node connected directly by a line.

**Answer: 7**

Figure 23 | Example from word search task.

### Wrapping Path Finding

**Cartesian**



**Direction Key:**  
R = Right  
L = Left  
Up = Up  
Down = Down

(A) L Up Up Up L Up R R R R

(B) L Up Up Up Up Down R Up R R

(C) L Up Up Up R R R R R

(D) L Up Up Up R Up R R Down

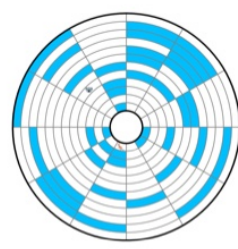
(E) L Up Up Up R R Up R Down

The kangaroo wants to reach the koala. It can move one cell at a time: Up, Down, Left (L), or Right (R). It cannot enter blue (water) cells. The top and bottom edges (thick black borders) are impassable, but the left and right edges wrap around (shown by dashed lines) -- moving left from the first column enters the last column, and vice versa. Which sequence of moves takes the kangaroo to the koala?

(A) (B) (C) (D) (E)

**Answer: C**

**Polar**



**Direction Key:**  
In = Inward  
Out = Outward  
CW = Clockwise  
CCW = Counter-Clockwise

(A) CCW Out Out Out CCW Out CW CW CW

(B) CCW Out Out Out In CW Out CW CW

(C) CCW Out Out Out CW CW CW CW

(D) CCW Out Out Out CW Out CW In

(E) CCW Out Out Out CW CW Out CW In

The kangaroo wants to reach the koala. It can move one cell at a time: Inward (In), Outward (Out), Clockwise (CW), or Counter-Clockwise (CCW). It cannot enter blue (water) cells. The thick black inner and outer circles are impassable boundaries, but the grid wraps around in the angular direction -- the kangaroo can move continuously clockwise or counter-clockwise. Which sequence of moves takes the kangaroo to the koala?

(A) (B) (C) (D) (E)

**Answer: C**

Figure 24 | Example from wrapping path finding task.

### Wrapping Navigation

**Cartesian**

**Grid Legend:**  
R=Right | L=Left  
Up=Up | Down=Down  
Rocks & Top/Bottom Edges STOP Movement | L/R Wrap

**Question Path Sequence:**  
Down Down L Up R R Up R R Up R R Down L Up R Down Down R R Down Down L Down Down

The Ant starts at the House. The black arrow line shows its path to the Bee. Rocks block movement. If a move command directs the Ant into a rock or a solid wall, it bumps into it, **STOPS COMPLETELY**, and ignores ALL remaining commands in the sequence. The board wraps horizontally (moving off the right edge brings the Ant to the left edge). Top and bottom edges are solid walls. If it instead attempts to follow the absolute movement sequence shown in the light yellow box, which animal does it permanently stop at?

- (A) Bee
- (B) Frog
- (C) Butterfly
- (D) Caterpillar
- (E) Ladybug
- (F) Snail

**Answer: B**

**Polar**

**Polar Legend:**  
CW=Clockwise | CCW=Counter-Clockwise  
OUT=Outward | IN=Inward  
Rocks/Edges STOP Movement completely.

**Question Path Sequence:**  
IN IN CCW OUT CW CW OUT OUT CW CW IN CCW CCW OUT CW IN IN CW CW IN IN CCW IN IN

The Ant starts at the House. The black arrow line shows its path to the Bee. Rocks block movement. If a move command directs the Ant into a rock or a solid wall, it bumps into it, **STOPS COMPLETELY**, and ignores ALL remaining commands in the sequence. If it instead attempts to follow the movement sequence shown in the light cyan box at the bottom, which animal does it permanently stop at?

- (A) Bee
- (B) Frog
- (C) Butterfly
- (D) Caterpillar
- (E) Ladybug
- (F) Snail

**Answer: B**

Figure 25 | Example from wrapping navigation task.